Neuron

Article

Gut-induced alpha-Synuclein and Tau propagation initiate Parkinson's and Alzheimer's disease co-pathology and behavior impairments

Graphical abstract

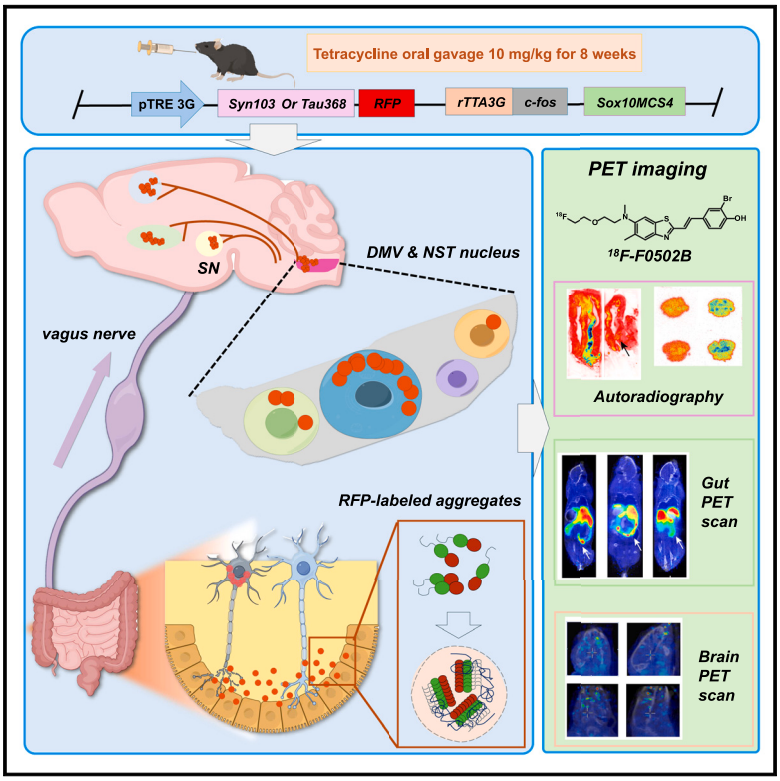

Highlights

- A gut-induced α-Syn and Tau co-pathology mouse model can spread into the brain
- Gut-derived pathology is propagated into the DMV and NTS at early stage
- Anxiety, cognitive, and motor behavioral impairments appear in a temporal manner
- The α-Syn PET tracer [^{18}F]-F0502B can detect α-Syn aggregates in the gut and brain

Authors

Jie Xiang, Jingrong Tang, Fei Kang, ..., Jing Wang, Shengxi Wu, Keqiang Ye

Correspondence

xj890119@fmmu.edu.cn (J.X.), shengxi@fmmu.edu.cn (S.W.), kq.ye@siat.ac.cn (K.Y.)

In brief

Xiang et al. establish a gut-inducible transgenic mouse model and detect that the gut-derived α-Syn or Tau pathology can propagate into the DMV or NTS and then to other brain regions. The α-Syn PET tracer [^{18}F]-F0502B can detect α-Syn aggregates in the gut and brain.

Xiang et al., 2024, Neuron *112*, 3585–3601
November 6, 2024
https://doi.org/10.1016/j.neuron.2024.08.003

CellPress

Neuron

CellPress

Article

Gut-induced alpha-Synuclein and Tau propagation initiate Parkinson's and Alzheimer's disease co-pathology and behavior impairments

Jie Xiang,[1,5,*] Jingrong Tang,[1,5] Fei Kang,[2,5] Jiajun Ye,[2] Yueying Cui,[1] Zhentao Zhang,[3] Jing Wang,[2] Shengxi Wu,[1,*] and Keqiang Ye[4,6,*]

[1]Department of Neurobiology, Fourth Military Medical University, Xi'an 710032, China
[2]Department of Nuclear Medicine, Xijing Hospital, Fourth Military Medical University, Xi'an 710032, China
[3]Department of Neurology, Renmin Hospital of Wuhan University, Wuhan 430060, China
[4]Faculty of Life and Health Sciences, Shenzhen University of Advanced Technology (SUAT), Chinese Academy of Sciences, Shenzhen, Guangdong 518055, China
[5]These authors contributed equally
[6]Lead contact
*Correspondence: xj890119@fmmu.edu.cn (J.X.), shengxi@fmmu.edu.cn (S.W.), kq.ye@siat.ac.cn (K.Y.)
https://doi.org/10.1016/j.neuron.2024.08.003

SUMMARY

Tau interacts with α-Synuclein (α-Syn) and co-localizes with it in the Lewy bodies, influencing α-Syn pathology in Parkinson's disease (PD). However, whether these biochemical events regulate α-Syn pathology spreading from the gut into the brain remains incompletely understood. Here, we show that α-Syn and Tau co-pathology is spread into the brain in gut-inducible SYN103$^{+/-}$ and/or TAU368$^{+/-}$ transgenic mouse models, eliciting behavioral defects. Gut pathology was initially observed, and α-Syn or Tau pathology was subsequently propagated into the DMV or NTS and then to other brain regions. Remarkably, more extensive spreading and widespread neuronal loss were found in double transgenic mice (Both) than in single transgenic mice. Truncal vagotomy and α-Syn deficiency significantly inhibited synucleinopathy or tauopathy spreading. The α-Syn PET tracer [^{18}F]-F0502B detected α-Syn aggregates in the gut and brain. Thus, α-Syn and Tau co-pathology can propagate from the gut to the brain, triggering behavioral disorders.

INTRODUCTION

Parkinson's disease (PD) is the second most common neurodegenerative disease and is a representative disease with aggregated α-Synuclein (α-Syn) inclusions in the brain, also called synucleinopathies.[1] α-Syn aggregation appears in the substantia nigra (SN) and triggers dopaminergic neuronal death, which is a pathological hallmark of PD. However, α-Syn aggregates can be detected in the gastrointestinal (GI) tract much earlier than in the brain.[2,3] Braak et al. hypothesize that α-Syn misfolding and aggregation probably begin in the enteric nervous system (ENS) and propagate *trans*-synaptically mainly via the vagus nerve in a self-promoting process.[4] In recent years, Braak's hypothesis has been supported by evidence showing that abnormal α-Syn accumulation in the ENS can be transported into the dorsal motor nucleus of the vagus (DMV), SN, and other higher brain regions.[3,5–9] Injecting recombinant or patient-derived pre-formed fibrils (PFFs) into the intestinal muscle layers of rodent models elicits aggregated protein propagation through the vagus nerve to the DMV and SN. However, there are some limitations to these models. The intestinal injection sites, depth, and doses are challenging to operate precisely, resulting in various propagating processes among different research groups. Most injection doses are several orders of magnitude higher than those present in the brain, which questions the accuracy in mimicking Parkinson's pathology.[10] Additionally, PFF preparation and purification primarily affect the final neurotoxicity and prion-like ability, which probably cause instability in experiments. Furthermore, these models cannot differentiate endogenous and gut-derived PFFs in the brain, which raises the question of whether gut-derived PFFs can directly enter the brain. Thus, there is an urgent need to develop an innovative mouse model that faithfully mimics the progression of PD pathology in the ENS. This model can further research in gut-brain transport and intervention treatments that can be tested to inhibit disease progression.

Mammalian asparagine endopeptidase (AEP) is a pH-dependent, endolysosomal cysteine protease that cleaves its substrates after asparagine residues.[11,12] In our previous studies, AEP cleaves Tau proteins in Alzheimer's disease (AD) and α-Syn in PD, producing Tau N368 and α-Syn N103 fragments that enhance prion-like protein aggregation and augment neurotoxicity in the brain.[12,13] We have shown that both α-Syn N103

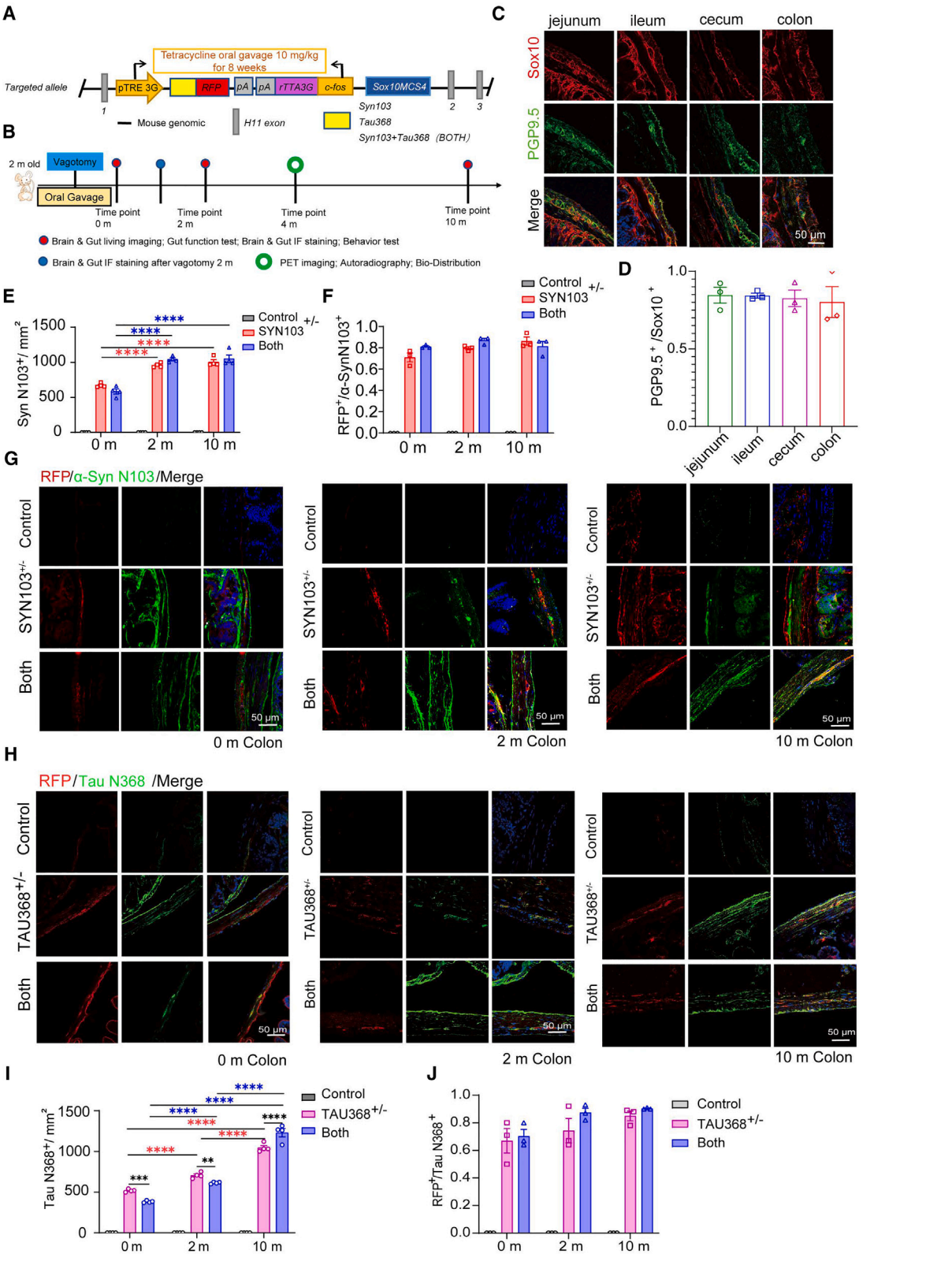

(legend on next page)

and Tau N368 are detectable in the gut biopsy tissues of PD and AD patients. These truncates co-localize in PD patient gut tissues.[8,14] In addition, Tau interacts with α-Syn and forms more compact neurotoxin fibrils, revealing enhanced propagation potential and neurotoxicity in an AEP-dependent manner. Injecting the intestine with α-Syn N103 and Tau N368 PFFs induces more PFFs to propagate through the vagus nerve than full-length PFFs, indicating that AEP-cleaved fragment PFFs may play a more crucial role in initiating PD progression from the ENS to the central nervous system (CNS).[8]

In the current study, we established gut-inducible transgenic mouse models, which induce α-Syn N103, Tau N368, or double fragment expression in the ENS with red fluorescent protein (RFP) tag without expression in the brain. After tetracycline induction, Tau N368 or Syn N103 truncates are expressed and aggregated in the enteric neurons in a time-dependent manner, accompanied with gut dysfunctions. RFP-tagged α-Syn N103 and Tau N368 appeared in many brain regions, with aggregated α-Syn and Tau propagating through the brainstem to the neocortex. Moreover, the induction of both fragments showed that more aggregates formed in the ENS and in brain regions with more tyrosine hydroxylase (TH) and total neuronal loss in the brain. The mouse models also displayed motor dysfunctions and cognitive impairment in a time-dependent manner, mimicking the behavioral disorders in PD patients. The Lewy-body-like pathology was validated by positron emission tomography (PET) imaging using [^{18}F]-labeled F0502B, a newly identified α-Syn PET tracer. Hence, our findings support the idea that gut PET-computed tomography (CT) imaging might be a potential measure to clinically diagnose prodromal PD patients with gut dysfunctions.

RESULTS

Establishment of α-Syn N103 and Tau N368 mouse models for tetracycline-inducible expression of transgenes in the ENS

SRY-box containing gene 10 (*Sox10*) is a critical transcription factor during neural-crest-derived cell development.[15] Because *Sox10* is expressed in the ENS, to establish inducible α-Syn N103 and Tau N368 transgenes selectively expressed in the ENS, we generated a Tet-on transgenic mouse line with *Sox10*-MCS4 (for multiple-species conserved sequences) as an enhancer with *c-Fos* minimal promotor and RFP coding sequences coupled with SYN103$^{+/-}$ or TAU368$^{+/-}$ or both genes (Figure 1A).[16–18] Because tetracycline barely penetrates the blood-brain barrier, it primarily induces transgene expression in the ENS neurons. To induce RFP-tagged target genes, we treated mice with 10 mg/kg tetracycline via oral gavage daily and consecutively for 8 weeks (0 months) and analyzed α-Syn N103 and Tau N368 expression at 0, 2, and 10 months after oral gavage (Figure 1B). To verify whether the *Sox10* enhancer induces enteric neuronal transgene expression, we stained SOX10 and PGP9.5, a marker for enteric neurons,[19] with their specific antibodies and observed that they co-localized in the enteric neurons (Figures 1C and 1D). Next, we performed GI tissue-section staining with RFP and α-Syn N103 and Tau N368 antibodies and observed that RFP signals co-localized with transduced α-Syn N103 or Tau N368 in SYN103$^{+/-}$, TAU368$^{+/-}$, and Both mice in the jejunum, ileum, cecum, and colon sections at 0, 2, and 10 months, indicating that these mouse lines induce α-Syn N103 and Tau N368 expression in the whole GI tract (Figures 1E–1J and S1A and S1B). To exclude the antibiotic-treatment-inducing-possible-interfering factors, we fed wild-type (WT) mice with tetracycline via oral gavage as a control group to examine the effects of antibiotic treatment on GI and observed no α-Syn aggregation or Tau aggregation in the gut or any abnormal behavioral defects (Figures S1C and S1D).

To assess whether the RFP signal localized in the enteric neurons, we co-stained RFP and PGP9.5 (the enteric marker in the myenteric nervous plexus) in the colon at different time points and observed that over 60% of enteric neurons were RFP positive (Figures S2A and S2B). To verify that induced α-Syn N103 and Tau N368 were indeed expressed in the enteric neurons, we conducted immunofluorescent (IF) staining and found similar results (Figures S2C–S2F). Choline acetyltransferase (ChAT)-positive neurons are investigated in multiple kinds of research on the gut-brain axis, and we applied a ChAT antibody to verify our staining results and observed similar results (Figures S3A–S3D). We also performed 3D whole-mount colon tissue staining

Figure 1. RFP signals co-localized with transduced α-Syn N103 or Tau N368 in SYN103$^{+/-}$, TAU368$^{+/-}$, and Both mice in the colon sections at 0, 2, and 10 months

(A) Schematic draw of transgenic mouse genome structure.

(B) Schematic draw of treatment and experiment timeline. 0, 2, 4, and 10 months presented the months post oral gavage (m.p.o.).

(C) Immunostaining showed Sox10 expression at 0 months in PGP9.5-positive cells. Scale bar, 50 μm.

(D) The statistics of (C). There were no statistically significant differences among the different GI regions; by one-way ANOVA.

(E) Quantification showed the increase of α-Syn N103 expression in a time-dependent manner. Results are shown as means ± SEM; $n = 4$ animals, each including 3 sections of mean cell numbers; ****$p < 0.0001$; by two-way ANOVA.

(F) Quantification showed RFP signal and α-Syn N103 mostly co-localized in the enteric cells. Results are shown as means ± SEM; $n = 3$ animals, each including 3 sections of mean cell numbers. There were no statistically significant differences among the SYN103$^{+/-}$ and Both groups at different time points by two-way ANOVA.

(G) 0, 2, and 10 months after oral gavage treatment, immunostaining showed RFP (red) and α-Syn N103 (green) co-localization in the colon. Scale bar, 50 μm.

(H) 0, 2, and 10 months after oral gavage treatment, immunostaining showed RFP (red) and Tau N368 (green) co-localization in the colon. Scale bar, 50 μm.

(I) Quantification showed the increase of Tau N368 expression in a time-dependent manner. Results are shown as means ± SEM; $n = 4$ animals, each including 3 sections of mean cell numbers; **$p < 0.01$, ****$p < 0.0001$; by two-way ANOVA.

(J) Quantification showed RFP signal and Tau N368 mostly co-localized in the enteric cells. Results are shown as means ± SEM; $n = 3$ animals, each including 3 sections of mean cell numbers. There were no statistically significant differences among the TAU368$^{+/-}$ and Both groups at different time points by two-way ANOVA.

See also Figures S1–S4 and Video S1.

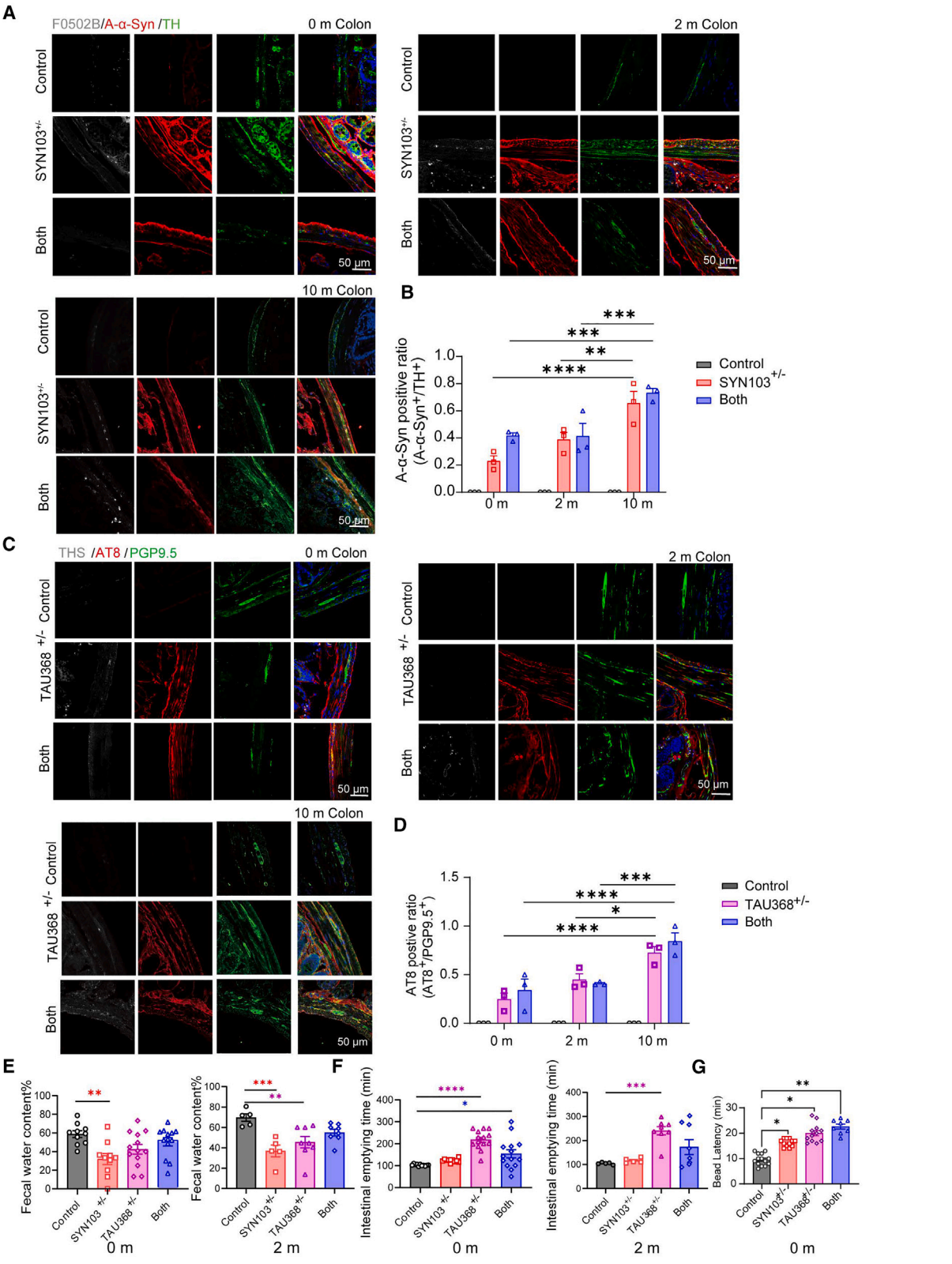

(legend on next page)

with α-Syn N103 and Tau N368 in SYN103$^{+/-}$, TAU368$^{+/-}$, and Both mouse colons and observed that these fragments were expressed along with the enteric plexus, further verifying that the mouse lines successfully transduce α-Syn and Tau fragment expression in the enteric neurons (Video S1). The quantitative analysis showed that the ENS-induced α-Syn N103 and Tau N368 were increased in a time-dependent manner, suggesting that induced α-Syn N103 and Tau N368 accumulated in the enteric plexus (Figures 1E–1J). Although the ENS contains a large number of glial cells, α-Syn N103 and Tau N368 truncates minorly co-localized with GFAP (glial fibrillary acidic protein)-positive cells, suggesting that induced α-Syn N103 and Tau N368 are predominantly expressed in neurons (Figures S3E–S3H).

To test whether α-Syn N103 and Tau N368 aggregate in the ENS, we performed IF co-staining with antibodies against aggregated α-Syn (A-α-Syn)/TH and AT8/PGP9.5, respectively. Evident aggregation in the colon increased in SYN103$^{+/-}$, TAU368$^{+/-}$, and Both mice compared with the control group from 0 to 10 months (Figures 2A–2D). Moreover, the whole-mount staining of the colon plexus showed similar findings: A-α-Syn and Tau were detected along the plexus fibers (Figure S4A). Remarkably, the neurons in the colon were prominently decreased in SYN103$^{+/-}$ and Both mice at 10 months, and a similar but relatively mild reduction occurred in TAU368$^{+/-}$ mice (Figure S4B). F0502B is an innovative α-Syn aggregation PET tracer with fluorescence. To validate α-Syn aggregation in the colon, we intravenously injected 10 mg/kg F0502B/PBS solution and sacrificed the mice 30 min later. *Ex vivo* staining showed that F0502B detected α-Syn aggregation in the colon (Figure 2A). Similarly, thioflavin-S (ThS) *ex vivo* staining detected Tau aggregation in the gut as well, strongly supporting the idea that induced α-Syn N103 and Tau N368 formed aggregates in the GI tract (Figure 2C).

Constipation is a prevalent symptom in up to 80% of PD patients.[20] α-Syn aggregation in the gut may result in constipation. Accordingly, we examined the fecal water contents and intestinal emptying time in control, SYN103$^{+/-}$, TAU368$^{+/-}$, and Both mice 8 weeks after tetracycline treatment (0 months) and 2 months after. Noticeably, SYN103$^{+/-}$ mice showed a prominent decrease in stool moisture after oral gavage (0 months), and the symptom became more severe 2 months after. TAU368$^{+/-}$ mice displayed evident fecal water content reduction with increasing GI tract transit time at 2 months (Figure 2E). Interestingly, intestinal emptying and bead latency assays showed Both mice displayed notable constipation after 8-week tetracycline induction (0 months) (Figures 2F and 2G). Thus, these findings suggest that induced α-Syn N103 and Tau N368 in the gut lead to α-Syn and Tau aggregation in the enteric neuronal plexus and elicit gut mobility defects.

Recent studies have identified Tau and α-Syn aggregation in several peripheral tissues, such as the heart, liver, retina, skin, and colon.[21–23] To determine whether our mouse models displayed peripheral Tau or α-Syn accumulation, we performed immunohistochemical (IHC) staining of lung, liver, heart, spleen, and kidney tissues in SYN103$^{+/-}$, TAU368$^{+/-}$, and Both mice. IHC staining revealed very weak α-Syn N103 immunoactivity in the heart, liver, and lung, whereas Tau N368 was barely detected in the heart, lung, and kidney (Figures S4C and S4D). However, the immunoactivities were trivial compared to the robust signals in the gut.

Spreading of α-Syn and Tau from the ENS to the brain

Evidence from human postmortem studies and PFF gut-injection PD mouse models suggest that α-Syn aggregates spread from the ENS to the DMV and subsequently propagate to different brain regions.[1,3,6,8] To examine whether aggregated α-Syn or Tau can be transported from the ENS to the CNS, we used α-Syn N103 and Tau N368 antibodies co-stained with RFP on the brain sections and mapped α-Syn N103 and Tau N368 brain distribution from 0 to 10 months. RFP signals co-localized with α-Syn N103, and Tau N368 appeared in the DMV and nucleus of the solitary tract (NTS) at 0 months in SYN103$^{+/-}$, TAU368$^{+/-}$, and Both mice, and they were progressively distributed to the locus coeruleus (LC), entorhinal cortex (EC), SN, and anterior cingulate cortex (ACC) regions at 2 months (Figures 3A–3D and S5A–S5C), indicating that α-Syn N103 and Tau N368 signals emanating from the ENS could be spread into different brain regions. Dotted pictures mapping from the whole-brain-slice imaging showed the brain distribution of α-Syn aggregates at 0 months. Both mice demonstrated more α-Syn N103 accumulation than SYN103$^{+/-}$ mice did (Figure 3E). Quantitative analysis of α-Syn N103-positive cells showed similar findings (Figure 3F). Interestingly, α-Syn N103 fibrils were spread to the hippocampus (HC) in Both mice but barely in SYN103$^{+/-}$ mice, indicating that α-Syn N103 and Tau N368 may form a complex and possess a more robust propagating capability in the brain at 10 months (Figure S5A). We made similar observations that Both mice exhibit

Figure 2. Induced α-Syn and Tau aggregated in a time-dependent manner in the enteric neurons by tetracycline treatment for 8 weeks and displayed GI dysfunction from 0 months

(A) Immunostaining showed F0502B (gray), A-α-Syn (red), and TH (green) co-localized in SYN103$^{+/-}$ and Both mouse colons. F0502B (gray), the α-Syn fluorescent probe; A-α-Syn (red), A-α-Syn antibody; TH (green), Tyrosine hydroxylase antibody marked catecholaminergic neurons. Scale bar, 50 μm.

(B) Quantification of TH-positive neurons with α-Syn aggregates ratio. Results are shown as means ± SEM; n = 3 animals, each including 3 sections of mean cell numbers; $^{**}p < 0.01$, $^{***}p < 0.001$, $^{****}p < 0.0001$; by two-way ANOVA.

(C) Immunostaining showed THS (gray), AT8 (red), and PGP9.5 (green) co-localized in TAU368$^{+/-}$ and Both mouse colons. THS, Thioflavin-S, marked as misfolded protein aggregations; AT8 (red), phospho-Tau (Ser202, Thr205) antibody as a marker for aggregated Tau; PGP9.5 (green), a marker for enteric neurons. Scale bar, 50 μm.

(D) Quantification of enteric neurons with Tau aggregates ratio. Results are shown as means ± SEM; n = 3 animals, each including 3 sections of mean cell numbers; $^{*}p < 0.05$, $^{****}p < 0.0001$; by two-way ANOVA.

(E–G) The effect of α-Syn and Tau aggregation in GI functions was evaluated. (E) Stool water contents; (F) intestinal transit time quantifications; (G) colonic transit time. Results are shown as means ± SEM; n = 5–13 animals; $^{*}p < 0.05$, $^{**}p < 0.01$, $^{***}p < 0.001$, $^{****}p < 0.0001$; by one-way ANOVA.

See also Figures S1E, S1F, S4A, and S4B.

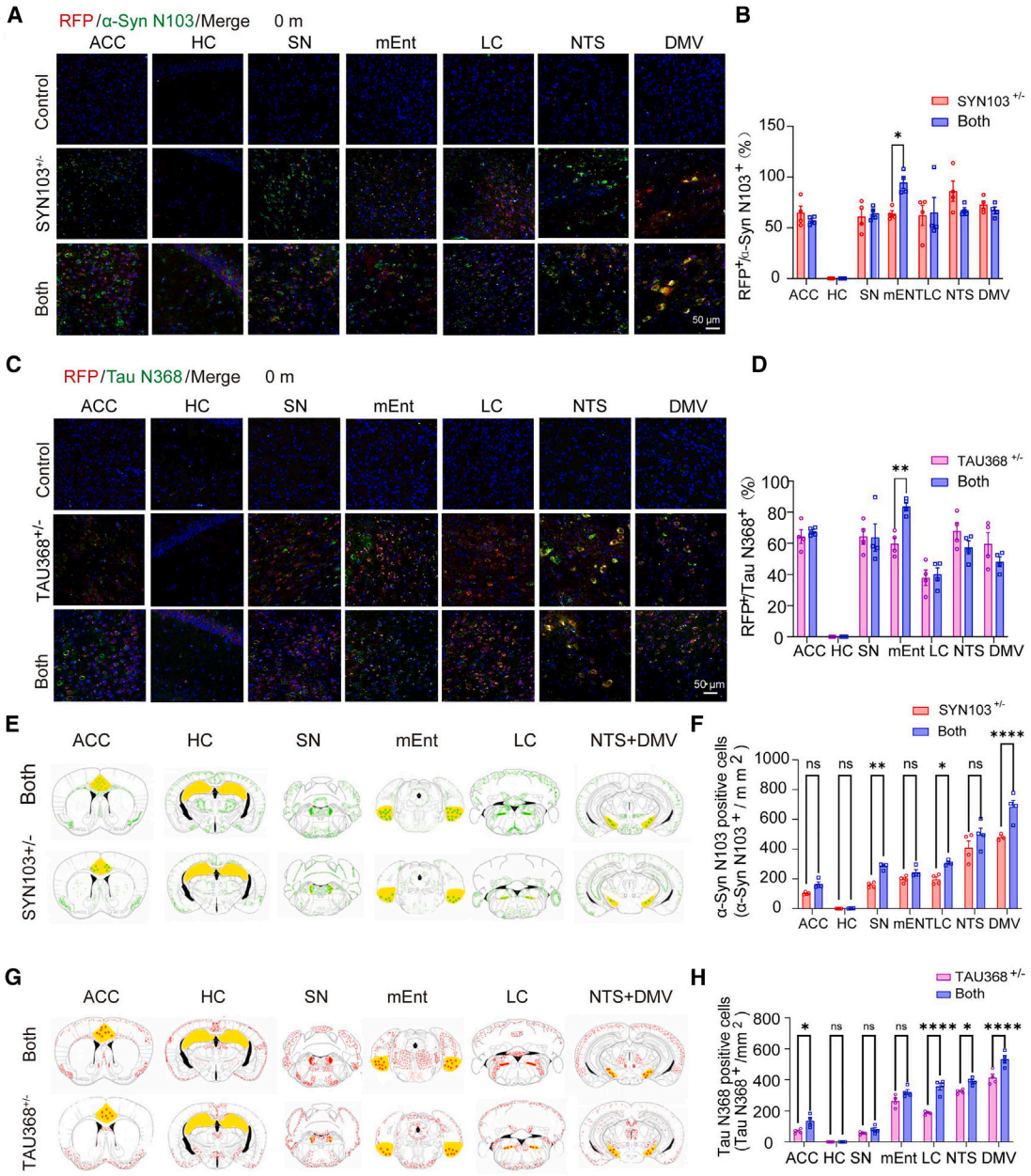

Figure 3. α-Syn N103 and Tau N368 brain distribution and quantification in SYN103$^{+/-}$, TAU368$^{+/-}$, and Both mice

(A) RFP and α-Syn N103 co-localized in SYN103$^{+/-}$ and Both mice brain regions at 0 months. Scale bar, 50 μm.

(B) RFP and α-Syn N103-positive cells were quantified. Data are shown as means ± SEM; $n = 3$ animals including 3 sections of each animal; $^{*}p < 0.05$; by one-way ANOVA.

(C) RFP and Tau N368 co-localized in TAU368$^{+/-}$ and Both mice brain regions at 0 months. Scale bar, 50 μm.

(D) RFP and Tau N368-positive cells were quantified. Data are shown as means ± SEM; $n = 4$ animals including 3 sections of each animal; $^{**}p < 0.01$; by one-way ANOVA.

(E) Dotted pictures showed α-Syn distribution in Both and SYN103$^{+/-}$ mouse brain regions at 0 months; the dotted pictures were drawn according to whole-brain section scanning of the image.

(F) α-Syn N103-positive cell density was quantified. Data are shown as means ± SEM; $n = 4$ animals including 3 sections of each animal; $^{*}p < 0.05$, $^{**}p < 0.01$, $^{****}p < 0.0001$, ns: no significance; by one-way ANOVA.

(G) Dotted pictures showed Tau N368 distribution in Both and TAU368$^{+/-}$ mouse brain regions at 0 months post oral gavage; the dotted pictures were drawn according to whole brain sections scanning image.

(H) Tau N368-positive cell densities were quantified. Data are shown as means ± SEM; $n = 4$ animals including 3 sections of each animal; $^{*}p < 0.05$, $^{****}p < 0.0001$; by one-way ANOVA.

See also Figures S5 and S6; Video S2.

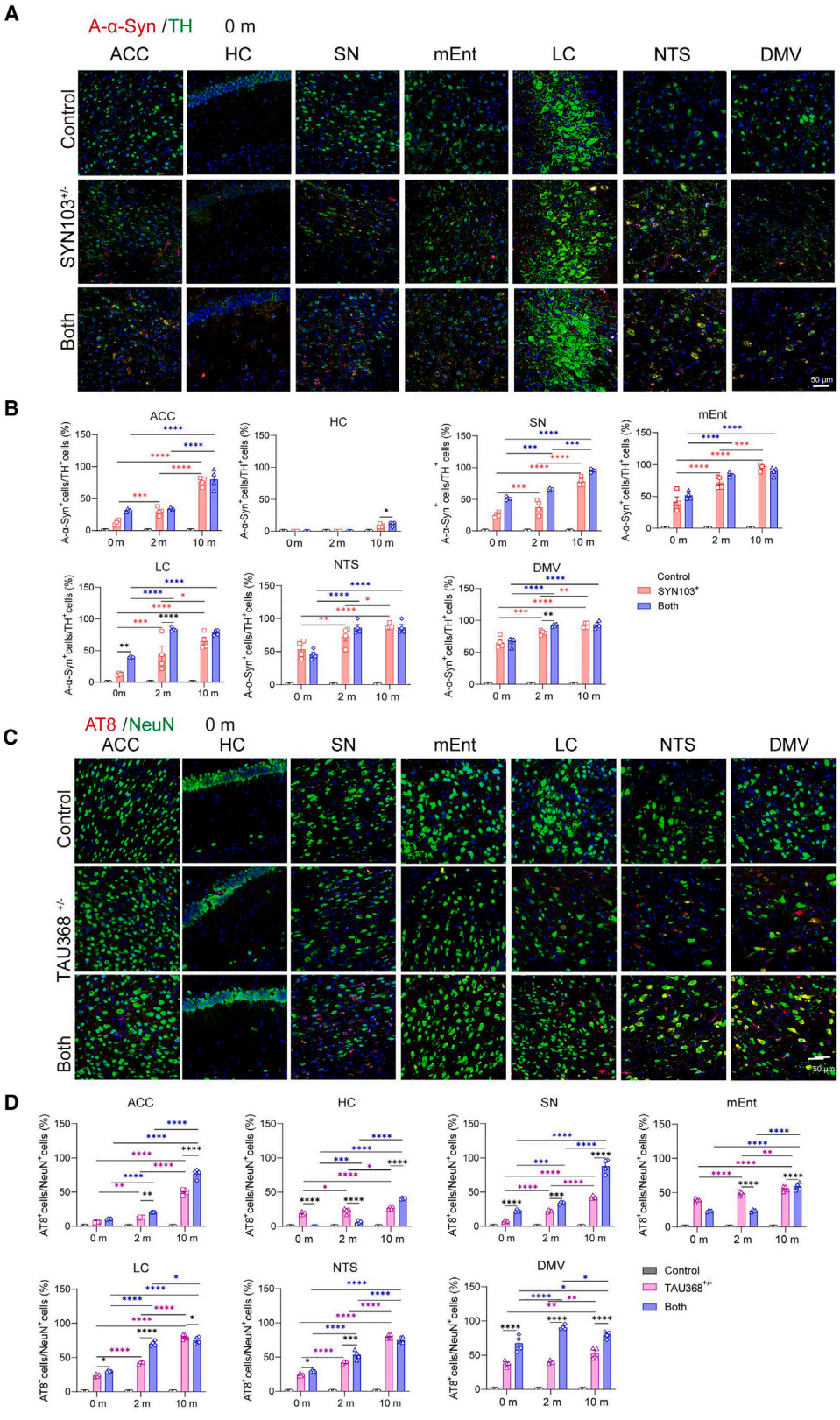

(legend on next page)

more Tau N368 spreading than TAU368$^{+/-}$ mice do at 0 months in the dotted pictures (Figure 3G). Accordingly, Tau N368 aggregates were distributed in more regions in Both mice than in TAU368$^{+/-}$ mice (Figure 3H). CC1, an anti-adenomatous polyposis coli clone, is a marker for mature oligodendrocytes in the brain. Since Sox10 is expressed in the oligodendrocyte lineage in the CNS, to further verify tetracycline-induced *sox10*-driven transgene specifically expressed in the gut but not the brain in our model, we administrated tetracycline to Both mice via oral gavage for 4 weeks and only observed RFP signals in the gut. However, there were no α-Syn N103 or Tau N368 signals detected in any of the brain regions, though CC1 pronouncedly labeled abundant oligodendrocytes (Figure S6), supporting the idea that this model specifically expresses α-Syn N103/Tau N368 in the ENS but not CNS. Moreover, we performed 3D SHIELD (short for "stabilization under harsh conditions via intramolecular epoxide linkages to prevent degradation," LifeCanvas Technologies) brain whole-mount α-Syn N103 and Tau N368 staining in Both, SYN103$^{+/-}$, and TAU368$^{+/-}$ mice at 10 months, and the spreading of α-Syn N103 and Tau N368 was detected in many brain regions (Video S2).

To further examine whether the aggregate spreading is similar to α-Syn N103 or Tau N368 signals, we performed A-α-Syn and AT8 co-staining with TH and NeuN (a neural marker) antibodies, respectively. Interestingly, IF results revealed that Both and SYN103$^{+/-}$ mice displayed aggregated α-Syn not only distributed to the NTS and DMV at 0 months but also spreading to the ACC and EC cortex (medial entorhinal cortex [mEnt]) (Figures 4A and 4B). Similarly, AT8-positive neurons were detected in the DMV, NTS, LC, and SN but barely in the ACC, which was also more extensive than Tau N368 signals in the brain at 0 months (Figures 4C and 4D), indicating that gut-derived Tau N368 and α-Syn N103 can act as seeds to induce endogenous α-Syn and Tau accumulation. The aggregates propagated in a time-dependent manner as the aggregation densities increased at 2 and 10 months (Figures S7 and S8). The A-α-Syn and AT8 signals in these brain regions were quantified and temporally increased (Figures 4B and 4D). Noticeably, Both mice revealed more aggregation in neurons than SYN103$^{+/-}$ and TAU368$^{+/-}$ mice did.

Dopaminergic neuronal loss in the SN is the hallmark of PD pathology. Consequently, we quantified TH-positive neurons in Both, SYN103$^{+/-}$, and control mice at 10 months (Figures S7D and S7E). TH neuronal density was significantly decreased in Both and SYN103$^{+/-}$ mice compared to those of control mice (Figure S7F), and we also observed that α-Syn N103 co-localized with TH neurons, indicating that TH neuronal loss may be attributed to induced α-Syn N103 spreading. We quantified neurons in the DMV, NTS, LC, and other brain regions and investigated whether A-α-Syn and Tau induced neuronal loss in different regions as PD and AD pathologies progressed. TH-positive neurons were decreased in the NTS and ACC at 0 months in Both and SYN103$^{+/-}$ mice, and the ACC, LC, SN, and NTS showed a more prominent reduction at 10 months compared to other regions (Figures S7A–S7C). Intriguingly, although the DMV is a critical brain region for α-Syn propagation from the ENS to the CNS, only mild TH neuronal loss was observed, even though the DMV exhibited a higher burden of α-Syn aggregation. Similarly, but differently, total neurons marked as NeuN-positive cells showed a significant decrease in the DMV, NTS, LC, EC, SN, and ACC at 10 months in Both and TAU368$^{+/-}$ mice, with more extensive and severe neuronal loss than TH-positive cells (Figures S8A–S8C). Furthermore, the LC and NTS displayed more neuronal loss in Both mice than in TAU368$^{+/-}$ mice, indicating that co-expression of α-Syn N103 and Tau N368 aggregates may induce more neurotoxicity in these regions. Notably, ChAT-positive neurons in NTS and DMV also showed significant propagation. The ratio of ChAT-positive neurons with aggregation was around 65%–85% (Figure S9). Interestingly, the TH cells and total neuron numbers only showed a mild reduction in the HC at 10 months, consistent with the relatively lower α-Syn and Tau distribution in HCs. Hence, these findings indicate that gut-derived α-Syn N103 and Tau N368 are spread in a time-dependent manner to the brain regions. The aggregation increases with α-Syn and Tau level augmentation, which also induces TH and neuronal loss in these regions.

Vagotomy decreased α-Syn and Tau aggregation in the brain

To test whether aggregated α-Syn and Tau are transported via the vagus nerve to the brain, we conducted truncal vagotomy 4 weeks after tetracycline treatment (Figures 1B and 5A). Two months after vagotomy, we performed IF to examine α-Syn and RFP expression in the brain. α-Syn aggregation decreased significantly in the DMV and NTS (Figures 5B–5D). Also, we observed ChAT-positive neuron loss in the vagotomy-treated group (Figure 5E). The A-α-Syn or AT8 signals were consistently decreased in the vagotomy group, accompanied by more TH- and NeuN-positive cells (Figures 5F–5H). Therefore, vagotomy decreases α-Syn and Tau aggregation in the brain.

To test whether the observed propagation in the mouse models needs endogenous α-Syn or Tau or merely the transport of α-Syn along the vagal nerve to the brain, we applied human α-Syn (S211)/Tau (HT7) marker staining to clarify the

Figure 4. α-Syn and Tau aggregates brain distribution and quantification in SYN103$^{+/-}$, TAU368$^{+/-}$, and Both mice

(A) Immunostaining showed α-Syn aggregation localized in TH-positive cells at 0 months post oral gavage in Both and SYN103$^{+/-}$ mouse brain regions. Scale bar, 50 μm.

(B) Quantification of α-Syn aggregation (marked as A-α-Syn) in TH-positive neuron density in different brain regions at different time points. Results are shown as means ± SEM; $n = 4$ animals including 3 sections; $^{*}p < 0.05$, $^{**}p < 0.01$, $^{***}p < 0.001$, $^{****}p < 0.0001$; by two-way ANOVA.

(C) Immunostaining showed Tau aggregation (marked as AT8) localized in TH-positive cells at 0 months in Both and TAU368$^{+/-}$ mouse brain regions. Scale bar, 50 μm.

(D) Quantification of Tau aggregation (marked as AT8) in neurons (marked as NeuN) density in different brain regions at different time points. Results are shown as means ± SEM; $n = 4$ animals including 3 sections; $^{*}p < 0.05$, $^{**}p < 0.01$, $^{***}p < 0.001$, $^{****}p < 0.0001$; by two-way ANOVA.

ACC, anterior cingulate cortex; HC, hippocampus; SN, substantia nigra; mEnt, medial entorhinal cortex; LC, locus coeruleus; NTS, the nucleus of the solitary tract; DMV, the dorsal motor nucleus of the vagus.

See also Figures S7–S10.

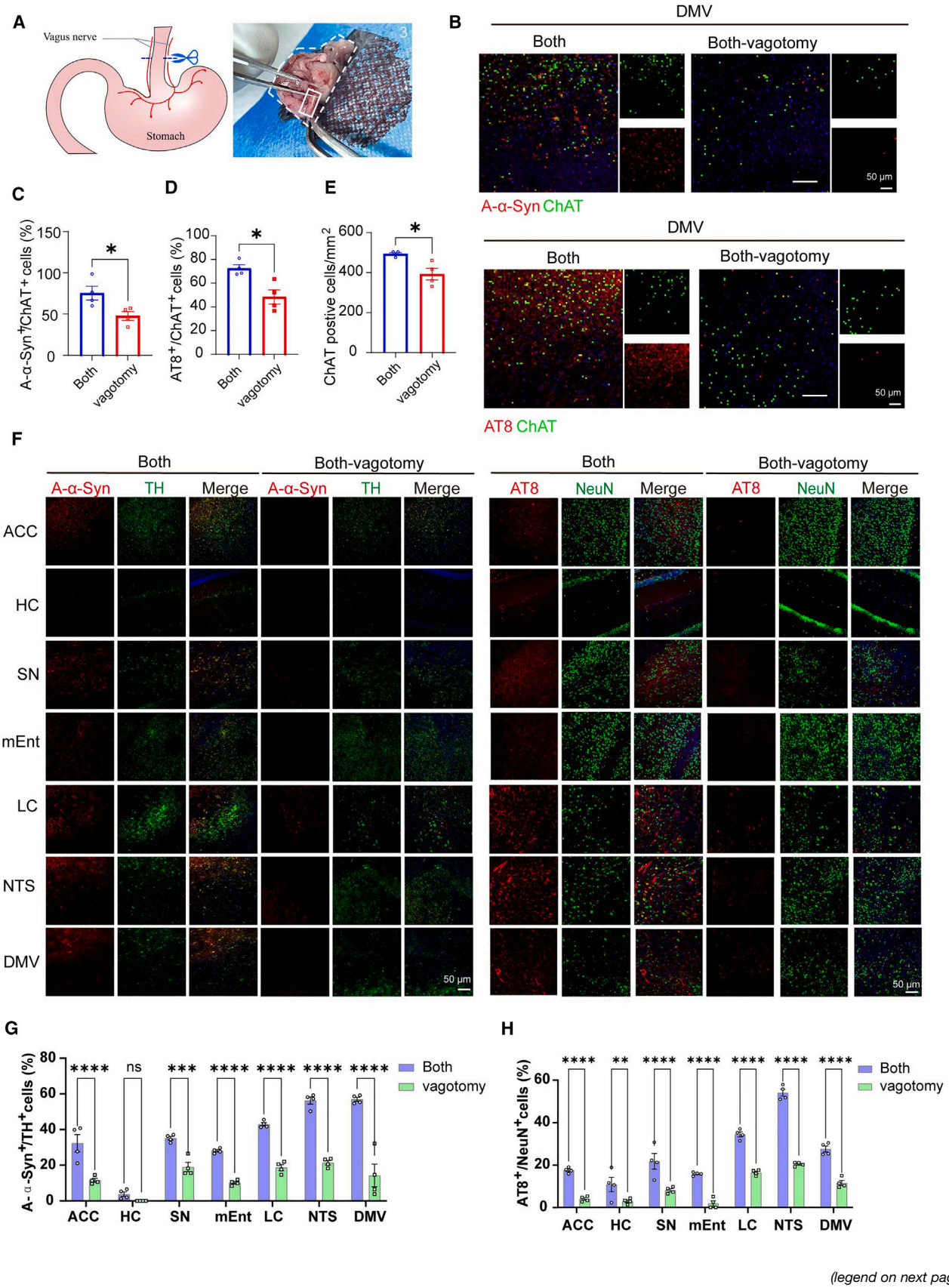

(legend on next page)

endogenous mouse proteins and the induced human fragments; similarly, we observed significant brain distribution from human fragments. However, RFP-positive signals were not completely co-localized with induced human fragments from the gut. This could be due to RFP tag shedding or non-specific staining (Figure S10). To further test the roles of endogenous α-Syn or Tau in fibril propagation, we extracted aggregated fibrils from the gut of 10-month SYN103 and TAU368 mice and injected them into the cecum and colon of α-Syn gene knockout (SNCA-KO) mice or Tau gene knockout (MAPT-KO) mice (1 μL each site) (Figure 6A). After 2 months, we tested aggregation in the injection site and observed demonstrable aggregation, indicating that endogenous α-Syn or Tau is not necessary for the formation of aggregates in the gut (Figures 6B–6E). Subsequently, we compared the aggregation propagation in the brain between KO and SYN103 or TAU368 mice. Clearly, the fibrils were much less distributed in KO mice as compared to those in the other two mice, indicating that endogenous α-Syn or Tau proteins are required for pathology propagation. Nonetheless, some of the minor α-Syn N103 fibrils were detected in different brain regions of α-Syn KO mice (SN, LC, and NTS), whereas Tau N368 fibrils were almost negligible in Tau KO brain, suggesting that endogenous Tau is absolutely required for the aggregates' propagation, and α-Syn is also implicated in the fibrils spreading from the gut to the brain, but not as much as Tau (Figures 6F–6I).

Behavioral dysfunctions in the mouse model

To explore whether gut-induced α-Syn N103 or Tau N368 aggregates elicit any behavioral disorders, we performed motor function, cognitive function, and depression-like anxiety assays at 0, 2, and 10 months after tetracycline treatment. The Rotarod test showed that only SYN103$^{+/-}$ and Both mice displayed motor deficits from 2 to 10 months, whereas the Tau N368 group remained comparable to the control group (Figure 7A). Moreover, the Morris water maze (MWM) showed that Both mice displayed a significantly increased escape latency compared to that of the control group, exhibiting substantial spatial learning deficits at 10 months. Additionally, Both mice spent less time in the quadrant area, suggesting memory impairment. However, SYN103$^{+/-}$ mice only showed memory impairment at 10 months. Notably, TAU368$^{+/-}$ mice revealed no defect at all (Figures 7B–7D). In addition, the novel object recognition test found that Both mice and SYN103$^{+/-}$ mice demonstrated a smaller amount of exploration time and recognition index for the novel objects at 0 months, displaying recognition memory deficits as early as 0 months and lasting up to 10 months, and TAU368$^{+/-}$ groups showed less novel object exploration starting at 2 months and lasting up to 10 months (Figure 7E), suggesting memory dysfunction. Furthermore, in the open field test, SYN103$^{+/-}$ mice revealed anxiety-like behavior starting at 0 months and lasting to 10 months. In contrast, Both mice displayed anxiety behavior only at 10 months (Figures S11A and S11B). The tail suspension test demonstrated that the SYN103$^{+/-}$ group revealed a longer immobility duration at 0 months, suggesting depression-like anxiety. TAU368$^{+/-}$ and Both mice also showed similar behavior starting at 2 and 10 months, respectively (Figure S11C). Hence, gut-induced α-Syn N103 or Tau N368 aggregates elicit different behavioral deficits after the pathology is propagated into the different brain regions.

Fluorescent living images detect α-Syn and Tau aggregation in the gut and brain

F0502B is a fluorescent probe used to detect α-Syn aggregation *in vitro* and *in vivo*. Accordingly, we conducted *in vivo* fluorescent imaging 15–20 min after intravenously injecting 10 mg/kg F0502B into SYN103$^{+/-}$ and Both mice. α-Syn aggregation was determined through quantitative fluorescence intensity under a detector with an emission wavelength of 520 nm, and SYN103$^{+/-}$ and Both mice showed time-dependent increases in fluorescent signals in the brain and gut in both *in vivo* and *ex vivo* experiments (Figure S12). Therefore, our data support the idea that α-Syn progressively aggregates in the gut and the brain.

^{18}F-F0502B detects α-Syn aggregation in the gut and brain

^{18}F-labeled F0502B has recently been identified as a promising radiotracer for imaging α-Syn inclusions in synucleinopathies.[24] To further investigate whether ^{18}F-F0502B detects α-Syn inclusions in the gut, we performed dynamic PET-CT scans using Both and SYN103$^{+/-}$ mice 4 months after tetracycline treatment. Preparation and physicochemical characterization of ^{18}F-F0502B were described in the STAR Methods and supplementary materials (Figure S13). ^{18}F-F0502B exhibits high lipophilicity (log D7.4 = 2.70 ± 0.41), and it was mainly excreted by the liver through the bile duct into the small intestine, and this might display the nonspecific signal in PET images. To avoid the

Figure 5. Immunostaining confirmed that α-Syn N103 and Tau N368 decreased in the brain regions after vagotomy at 2 months

(A) Surgery diagram and photos of vagotomy procedures.

(B) Immunostaining showed that α-Syn or Tau aggregates decreased significantly in ChAT-positive neurons after vagotomy at 2 months. Scale bar, 50 μm.

(C) Quantifications of α-Syn aggregates in ChAT-positive neurons. Results are shown as means ± SEM; $n = 4$ animals including 3 sections; $^{*}p < 0.05$ by Student's t test.

(D) Quantifications of Tau aggregates in ChAT-positive neurons. Results are shown as means ± SEM; $n = 4$ animals including 3 sections; $^{*}p < 0.05$ by Student's t test.

(E) Quantifications of ChAT-positive neuron densities. Results are shown as means ± SEM; $n = 4$ animals including 3 sections; $^{*}p < 0.05$ by Student's t test.

(F) Both mice after vagotomy at 2 months showed α-Syn and Tau aggregation decreasing in the brain regions. Left, A-α-Syn (green) and RFP (red) co-stained in different brain sections of Both and Both-vagotomy groups. Right, AT8 (green) and RFP (red) co-stained in different brain sections of Both and Both-vagotomy groups. Scale bar, 50 μm.

(G) Quantifications of α-Syn aggregates in TH-positive neurons in different brain regions. Results are shown as means ± SEM; $n = 4$ animals including each 3 sections; $^{***}p < 0.001$, $^{****}p < 0.0001$; by two-way ANOVA.

(H) Quantifications of Tau aggregates in neurons at different brain regions. Results are shown as means ± SEM; $n = 4$ animals including each 3 sections; $^{***}p < 0.001$, $^{****}p < 0.0001$; by two-way ANOVA.

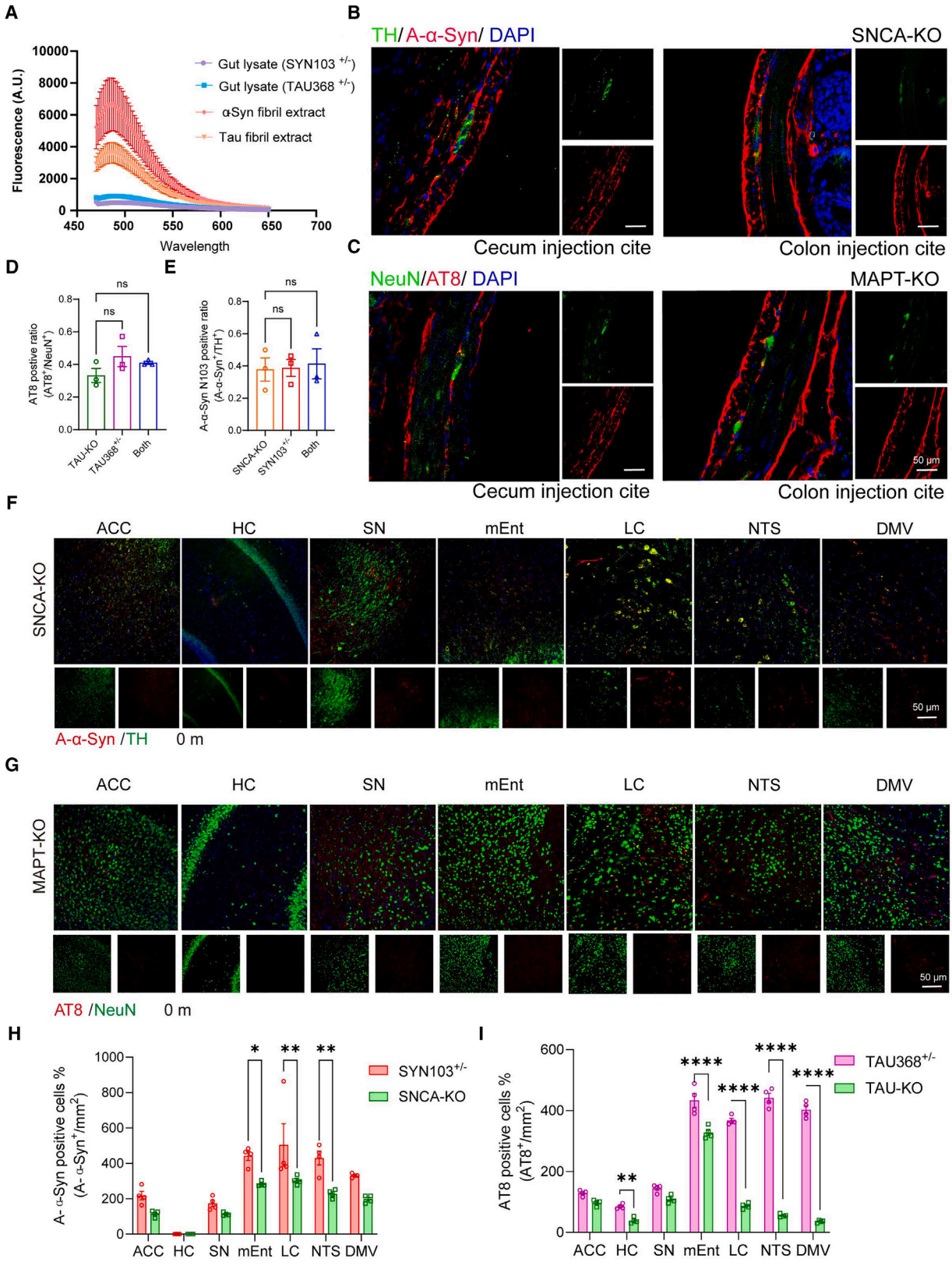

(legend on next page)

influence of this nonspecific signal in the detection of α-Syn target within the intestinal wall, we monitored the dynamic change of PET signals after ^{18}F-F0502B injection in control mice and found that 14–20 min post-injection (p.i.) would be the optimal observation window time to monitor pathogenic α-Syn signals within the intestinal wall. PET imaging demonstrated that Both and SYN103$^{+/-}$ mice displayed a significant increase in the distal intestine during 14–20 min after intravenous (i.v.) injection with ^{18}F-F0502B (Figure 8A, Video S3). We scaled the image to a standardized uptake value (SUV) in the distal intestine, which showed much higher signals in Both and SYN103$^{+/-}$ mice than those in the control group during this time window (Figure 8B).

To further determine whether ^{18}F-F0502B detects propagated α-Syn inclusions in the brain by PET imaging, we performed the brain PET-CT and analyzed ^{18}F-F0502B uptake at 30 min (Figure S13E). Although we observed ^{18}F-F0502B signals in the brains of Both and SYN103$^{+/-}$ mice, the imaging could not clearly show a specific brain region, which might be due to relatively lower α-Syn inclusions than other synucleinopathy mouse models and lack of micro-PET/CT resolution. To further verify that ^{18}F-F0502B detects α-Syn aggregates in the gut and the brain, we performed autoradiography with the GI tract and brain slices and quantitatively analyzed the uptake of major organs, different GI tract parts, and brain regions by biodistribution. The results showed that the highest uptake was in the jejunum due to bile duct excretion. We found that ^{18}F-F0502B selectively detected α-Syn aggregation in Both and SYN103$^{+/-}$ mice in the distal intestine, cecum, and colon, especially in the ileum (Figures 8C and 8E). Compared to PET/CT imaging, autoradiography and biodistribution clearly show uptake differences between brain regions (Figure S13E). Strikingly, nearly all the brain regions in Both mice showed much higher uptake compared to those in the control group. SYN103$^{+/-}$ mice showed a similar pattern but only slightly higher than the control group with higher ^{18}F-F0502B uptake in the medulla, which included LC, NTS, and DMV regions (Figures 8D and 8F). These results support the idea that ^{18}F-F0502B detects α-Syn inclusions in the gut and monitors α-Syn propagation to the brain.

DISCUSSION

The present study shows that the transduced α-Syn and Tau aggregates are transported from the intestinal-colon tract stereotypically via the vagus nerve into the brain. Notably, α-Syn N103 and Tau N368 double knock in after conditional gut-specific induction displayed more potent propagation capabilities. AEP-cleaved α-Syn N103 and Tau N368 fragments potently associate with each other in the gut, propagate into the brain, and act as seeds to induce endogenous α-Syn and Tau to form aggregates. They can transmit in anatomically interconnected brain regions, leading to motor dysfunction, cognitive impairment, and psychological behavioral disorders in a time-dependent manner. We detected α-Syn aggregation in the gut and brain using a Lewy-body-like specific F0502B probe and observed higher fluorescent signals *in vivo* and *ex vivo*. Furthermore, ^{18}F-labeled F0502B detects α-Syn inclusions in the gut under PET-CT scans, demonstrating that α-Syn aggregates in the gut might be a critical prodromal symptom relevant to PD pathogenesis. Therefore, detection of gut-derived α-Syn aggregates might be a promising early diagnostic strategy for PD with gut-related prodromal symptoms.

Previous clinical studies have confirmed that α-Syn and Tau accumulate in the gut,[10,23,25–28] and a series of studies attempted to establish α-Syn or Tau transportation from the ENS to the CNS models, which might investigate Braak's hypothesis.[1,6,8,9,14,29,30] Numerous models were explored by injecting PFFs into different GI tract sites, and the pathology was monitored in the vagus nerve and brain distributions. However, the differences among the PFF strains, doses, and injection sites made it difficult to conclude that gut-derived α-Syn accumulation can cause PD-like pathology in mice. To circumvent these variations, we established transgenic mice, which induce toxic α-Syn N103 and Tau N368 fragments expressed in the entire ENS, which makes the model more stable and practical in experiments. We have reported that both α-Syn N103 and Tau N368 are detectable in the gut biopsy tissues from PD and AD patients. They co-localize in the gut in PD patients. Furthermore, we have reported that Tau interacts with α-Syn and forms a denser neurotoxin complex, demonstrating more propagation potential and neurotoxic activities than full-length counterparts, for which AEP is indispensable.[8] C/EBPβ/AEP signaling is activated in an age-dependent manner in PD and mediates α-Syn pathology in the gut and brain.[31] Interestingly, intrastriatal injection of α-Syn N103/Tau N368 PFFs promotes endogenous α-Syn aggregates in the proximal colon,[32] suggesting that these fibrils could spread in an antegrade propagation manner along the

Figure 6. SNCA-KO mice or MAPT-KO mice injected with extracted aggregated fibrils showed aggregation formation in the injection site in the gut, and minor aggregates were detected in the brain regions

(A) Aggregate ThT binding assay. Aggregates extracted from SYN103$^{+/-}$ and TAU368$^{+/-}$ mouse gut tissue. α-Syn N103 and Tau N368 aggregation (0.7 μM) was assessed with ThT assays. Gut lysates were set as the control group.

(B and C) Immunostaining showed A-α-Syn and TH/NeuN co-localized in SNCA-KO mice or MAPT- KO mice injection site. Scale bar, 50 μm.

(D) Quantification of neurons with Tau aggregate ratio compared between MAPT-KO, Both, and TAU368$^{+/-}$ mice. Results are shown as means ± SEM; n = 3 animals, each including 3 sections of mean cell numbers; by two-way ANOVA.

(E) Quantification of TH-positive neurons with α-Syn aggregate ratio between SNCA-KO, Both, and SYN103$^{+/-}$ mice. Results are shown as means ± SEM; n = 3 animals, each including 3 sections of mean cell numbers by two-way ANOVA.

(F) Immunostaining showed α-Syn aggregation localized in TH-positive cells in SNCA-KO mouse brain regions. Scale bar, 50 μm.

(G) Immunostaining showed Tau aggregation localized in neurons in MAPT-KO mouse brain regions. Scale bar, 50 μm.

(H) Quantification of α-Syn aggregation (marked as A-α-Syn) density in different brain regions compared between SNCA-KO and SYN103$^{+/-}$ mice. Results are shown as means ± SEM; n = 4 animals including 3 sections; $^{*}p < 0.05$, $^{**}p < 0.01$; by two-way ANOVA.

(I) Quantification of Tau aggregation (marked as AT8) density in different brain regions compared between MAPT-KO and TAU368$^{+/-}$ mice. Results are shown as means ± SEM; n = 4 animals including 3 sections; $^{**}p < 0.01$, $^{****}p < 0.0001$; by two-way ANOVA.

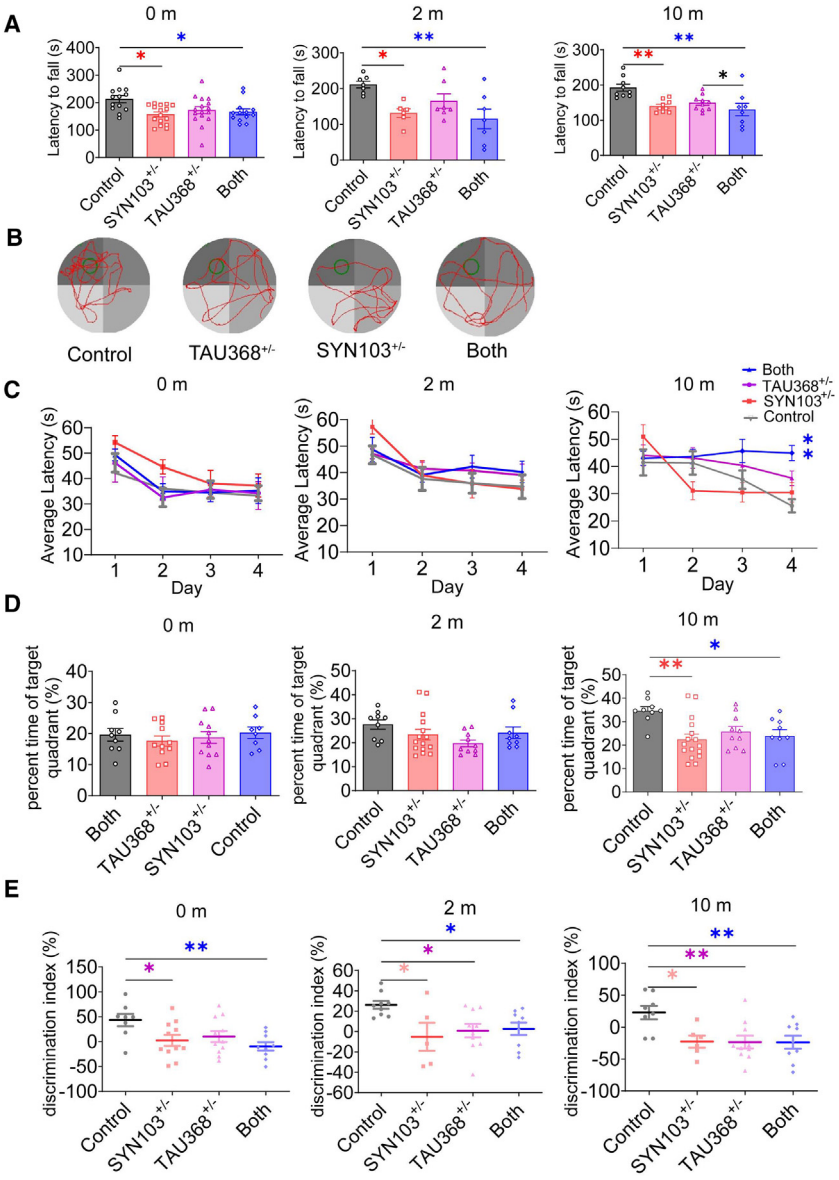

Figure 7. The motor and cognitive behavior tests with SYN103$^{+/-}$, TAU 368 $^{+/-}$, and Both mice

All behavioral tests were conducted at three-time points: 0 months after oral gavage (m.p.o.), 2 months, and 10 months.

(A) Rotarod test showed transgenic mice displayed motor deficit in a time-dependent manner.

(B) Representative swimming trajectory of mice at 0 months.

(C) MWM test showed Both mice exhibited different average latency compared to those of the control group at 10 months.

(D) MWM test showed SYN103 $^{+/-}$ and Both mice exhibited memory deficiency at 10 months.

(E) Novel object recognition test showed SYN103 $^{+/-}$ and Both mice revealed memory deficits as early as 0 months and lasted to 10 months, while TAU368 $^{+/-}$ mice showed deficits starting at 2 months.

Results are shown as means ± SEM; n = 6–16 animals in each group; $^{*}p < 0.05$, $^{**}p < 0.01$; by one-way ANOVA.

See also Figure S11.

vagus nerve into the gut. In this study, we observed weak α-Syn N103 and Tau N368 immunoactivity in peripheral organs, such as the liver and lung. Some clinical studies detected these signals in peripheral tissues in PD patients, and it is difficult to identify whether they directly come from the gut or from the brain along the neural projection or are indirectly affected by circulation. Clearly, further investigation is warranted.

To determine whether co-expression of α-Syn and Tau results in more abundant brain distributions, we compared the pathology of Both, SYN103$^{+/-}$, and TAU368$^{+/-}$ mice and observed that Both mice showed earlier and denser A-α-Syn distributions as well as Tau phosphorylation. However, the aggregation in the ENS did not show much difference among the three groups but displayed more PGP9.5-positive neuronal loss in the ENS (Figure S4B). It is worth noting that GI dysfunction was inconsistent with ENS TH neuronal loss. TAU368$^{+/-}$ mice showed more severe GI motor dysfunction, indicating that these disorders are not only caused by local neuronal loss but also by other factors. Clinical studies have indicated that preclinical AD is associated with Tau independent of memory deficits.[33,34] Consistent with the clinical studies, we observed that Both and TAU368$^{+/-}$ mice exhibited earlier spatial and cognitive memory impairment than SYN103$^{+/-}$ mice did, further suggesting that our mouse models exhibit more similarities with human tauopathy diseases. Motor dysfunction is a critical symptom of PD. We also examined motor behaviors and SN TH neuronal loss, which is closely related to motor disorders (Figures 7, S7D–S7F and S11). Interestingly, only SYN103$^{+/-}$ mice displayed motor dysfunction after tetracycline induction, although Both mice showed comparable TH loss in the SN region. These findings may explain why SYN103$^{+/-}$ mice mainly exhibit TH loss, which is relatively limited to the dopaminergic neuron system, inducing an imbalance in dopamine homeostasis by enhancing the dopamine indirect pathway. However, Both mice showed more extensive neuronal loss, so they may not display a more obvious motor function disorder.

Because α-Syn accumulation is a critical prodromal pathology in PD many years before motor disorders, it is clinically significant to detect gut α-Syn accumulation.[26,35–37] For now, no specific PD PET tracers target gut α-Syn accumulation. To assess whether ^{18}F-labeled F0502B can detect α-Syn inclusions in the gut, we performed PET scans of Both and SYN103$^{+/-}$ mice. Noticeably, although the intestinal metabolic signals interfered with the imaging, we still managed to pin down the time window to monitor the distal intestinal pathological signals.

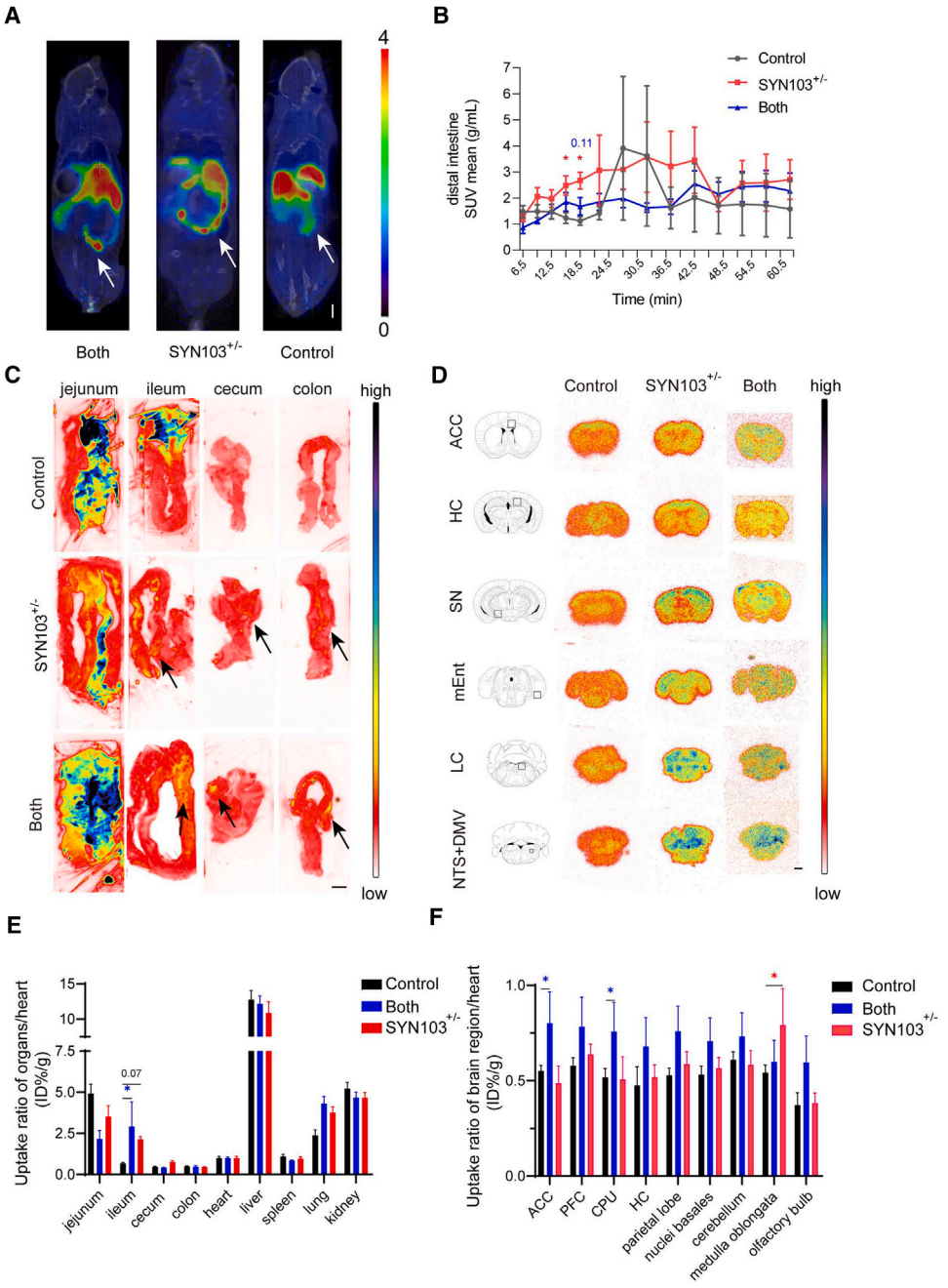

Figure 8. Visualization and quantitative analysis of α-Syn in the gut and brain using ^{18}F-F0502B

(A) *in vivo* micro-PET/CT imaging, showed that ^{18}F-F0502B detected distal intestine α-Syn signals at 17–20 min in Both and SYN103$^{+/-}$ mice at 4 months. Scale bar, 5 mm.

(B) The standardized uptake value (SUV)-time curve of the distal intestine in micro-PET/CT imaging after injection of ^{18}F-F0502B. Each point represents the average of the 3 subjects. Results are shown as means ± SEM; $n = 3$ animals in each group. $^{*}p < 0.05$; by one-way ANOVA.

(C) Autoradiography showed the distal intestine, cecum, and colon revealed more *ex vivo* ^{18}F-F0502B signals in Both than in SYN103$^{+/-}$ mice. Scale bar, 5 mm.

(D) Autoradiography showed *ex vivo* ^{18}F-F0502B signal distribution in different brain regions in Both and SYN103$^{+/-}$ mice. Scale bar, 1 mm.

(E and F) Bio-distribution studies showed ^{18}F-F0502B distributed in different organs (E) and brain regions (F). Each point represents the average of the 3 subjects. Results are shown as the ratio with heart uptake, means ± SEM; $n = 3$ independent experiments. $^{*}p < 0.05$; by one-way ANOVA.

PFC, prefrontal cortex; CPU, caudate putamen nucleus.

See also Figures S12 and S13, Video S3.

Furthermore, autoradiography and biodistribution assays confirmed that ^{18}F-F0502B can be used to detect α-Syn accumulation *ex vivo*. Interestingly, SYN103$^{+/-}$ mice revealed more obvious signals than Both mice, possibly due to the conformational change of α-Syn in the α-Syn-Tau complex inhibiting the interaction of F0502B with aggregated α-Syn in Both mice. Our findings support the idea that ^{18}F-F0502B is a promising PET tracer to detect GI α-Syn accumulation *in vivo* (Figure 8). However, the brain PET imaging strategy still needs to be improved. Together, our study strongly supports the idea that gut-derived α-Syn and Tau can be directly transported into the brain via the vagus nerve and induce neuronal loss in the gut and the brain, initiating behavioral impairments related to PD and AD. Therefore, gut-derived α-Syn accumulation is a promising target in the clinic for the diagnosis of prodromal PD. Conceivably, early therapeutic intervention may prevent pathological Lewy body spreading from the gut into the brain to cure devastating disease.

RESOURCE AVAILABILITY

Lead contact

Further information and requests for resources and reagents should be directed to and will be fulfilled by the lead contact, Keqiang Ye (kq.ye@siat.ac.cn).

Materials availability

This study did not generate new unique reagents.

Data and code availability

- All data reported in this paper will be shared by the lead contact upon request.
- The original statistical data has been deposited at https://data.mendeley.com/datasets/dfmw8fvxc2/1 and will be publicly available on 25 October 2024.
- Any additional information required to reanalyze the data reported in this paper is available from the lead contact upon request.

ACKNOWLEDGMENTS

This work was supported by the National Natural Science Foundation of China (no. 82394431 and no. 32330040 to K.Y., no. 82221001 to S.W., no. 92259304 and no. 91959208 to J.W., no. 82122033 to F.K., and no. 82001127 to J.X.), STI2030-Major Projects 2021ZD0201005 to S.W., the National Postdoctoral Program for Innovative Talents (BX20200155) to J.X., the Interdisciplinary research project of Xijing Hospital XJZT24JC15 to J.X. and F.K., and the Shaanxi Science and Technology rising star (2024ZC-KJXX-114) to J.X. The project was also supported by the Key Laboratory of Biomedical Imaging Science and System, Chinese Academy of Sciences, to K.Y. We thank Sundia Inc. for F0502B chemical synthesis support and the Animal research center of Fourth Military Medical University for animal care.

AUTHOR CONTRIBUTIONS

K.Y., S.W., and J.X. conceived the project, designed the experiments, analyzed the data, and wrote the manuscript. J.X., J.T., and F.K. performed most of the experiments. J.X., J.T., and Y.C. performed animal surgery, IF staining, histochemistry staining, and animal behavior tests and analysis. J.T. and Y.C. prepared brain and intestine samples and quantifications of images. J.Y., F.K., and J.T. conducted the microPET imaging, radiolabeling of ^{18}F-F0502B, autoradiography, and biodistribution. J.W., Z.Z., and S.W. assisted with data analysis and interpretation and critically read the manuscript. All of the authors are involved in analyzing the data and contributed to manuscript discussion and editing.

DECLARATION OF INTERESTS

K.Y. is a co-founder of Shanghai Braegen Pharmaceuticals, Inc., which licensed the PET tracer patent from Emory University. No data are sponsored by the company.

STAR★METHODS

Detailed methods are provided in the online version of this paper and include the following:

- KEY RESOURCES TABLE
- EXPERIMENTAL MODEL AND SUBJECT DETAILS
  - Mice
- METHOD DETAILS
  - Immunofluorescence staining
  - Immunohistochemical staining
  - Cell quantification
  - Stereological cell quantification
  - 3D-whole-brain and colon imaging
  - Gastrointestinal motility assays
  - Vagotomy
  - Rotarod test
  - Tail suspension test
  - Novel object recognition test
  - Water maze test
  - Open field test
  - *In vivo* and *ex vivo* imaging of the brain and the GI tract
  - Radiochemistry
  - Lipophilicity and *in vitro* stability
  - Micro-PET/CT imaging
  - Autoradiography
  - Biodistribution
- QUANTIFICATION AND STATISTICAL ANALYSIS

SUPPLEMENTAL INFORMATION

Supplemental information can be found online at https://doi.org/10.1016/j.neuron.2024.08.003.

Received: October 10, 2023
Revised: May 30, 2024
Accepted: August 7, 2024
Published: September 5, 2024

REFERENCES

1. Kim, S., Kwon, S.H., Kam, T.I., Panicker, N., Karuppagounder, S.S., Lee, S., Lee, J.H., Kim, W.R., Kook, M., Foss, C.A., et al. (2019). Transneuronal Propagation of Pathologic alpha-Synuclein from the Gut to the Brain Models Parkinson's Disease. Neuron *103*, 627–641.e7. https://doi.org/10.1016/j.neuron.2019.05.035.
2. Hawkes, C.H., Del Tredici, K., and Braak, H. (2010). A timeline for Parkinson's disease. Parkinsonism Relat. Disord. *16*, 79–84. https://doi.org/10.1016/j.parkreldis.2009.08.007.
3. Braak, H., de Vos, R.A.I., Bohl, J., and Del Tredici, K. (2006). Gastric alpha-synuclein immunoreactive inclusions in Meissner's and Auerbach's plexuses in cases staged for Parkinson's disease-related brain pathology. Neurosci. Lett. *396*, 67–72. https://doi.org/10.1016/j.neulet.2005.11.012.
4. Del Tredici, K., and Braak, H. (2016). Review: Sporadic Parkinson's disease: development and distribution of alpha-synuclein pathology. Neuropathol. Appl. Neurobiol. *42*, 33–50. https://doi.org/10.1111/nan.12298.
5. Holmqvist, S., Chutna, O., Bousset, L., Aldrin-Kirk, P., Li, W., Björklund, T., Wang, Z.Y., Roybon, L., Melki, R., and Li, J.Y. (2014). Direct evidence of Parkinson pathology spread from the gastrointestinal tract to the brain in

rats. Acta Neuropathol. *128*, 805–820. https://doi.org/10.1007/s00401-014-1343-6.

6. Challis, C., Hori, A., Sampson, T.R., Yoo, B.B., Challis, R.C., Hamilton, A.M., Mazmanian, S.K., Volpicelli-Daley, L.A., and Gradinaru, V. (2020). Gut-seeded α-synuclein fibrils promote gut dysfunction and brain pathology specifically in aged mice. Nat. Neurosci. *23*, 327–336. https://doi.org/10.1038/s41593-020-0589-7.
7. Manfredsson, F.P., Luk, K.C., Benskey, M.J., Gezer, A., Garcia, J., Kuhn, N.C., Sandoval, I.M., Patterson, J.R., O'Mara, A., Yonkers, R., and Kordower, J.H. (2018). Induction of alpha-synuclein pathology in the enteric nervous system of the rat and non-human primate results in gastrointestinal dysmotility and transient CNS pathology. Neurobiol. Dis. *112*, 106–118. https://doi.org/10.1016/j.nbd.2018.01.008.
8. Ahn, E.H., Kang, S.S., Liu, X., Chen, G., Zhang, Z., Chandrasekharan, B., Alam, A.M., Neish, A.S., Cao, X., and Ye, K. (2020). Initiation of Parkinson's disease from gut to brain by delta-secretase. Cell Res. *30*, 70–87. https://doi.org/10.1038/s41422-019-0241-9.
9. Uemura, N., Yagi, H., Uemura, M.T., Hatanaka, Y., Yamakado, H., and Takahashi, R. (2018). Inoculation of alpha-synuclein preformed fibrils into the mouse gastrointestinal tract induces Lewy body-like aggregates in the brainstem via the vagus nerve. Mol. Neurodegener. *13*, 21. https://doi.org/10.1186/s13024-018-0257-5.
10. Travagli, R.A., Browning, K.N., and Camilleri, M. (2020). Parkinson disease and the gut: new insights into pathogenesis and clinical relevance. Nat. Rev. Gastroenterol. Hepatol. *17*, 673–685. https://doi.org/10.1038/s41575-020-0339-z.
11. Zhang, Z., Tian, Y., and Ye, K. (2020). delta-secretase in neurodegenerative diseases: mechanisms, regulators and therapeutic opportunities. Transl. Neurodegener. *9*, 1. https://doi.org/10.1186/s40035-019-0179-3.
12. Zhang, Z., Song, M., Liu, X., Kang, S.S., Kwon, I.S., Duong, D.M., Seyfried, N.T., Hu, W.T., Liu, Z., Wang, J.Z., et al. (2014). Cleavage of tau by asparagine endopeptidase mediates the neurofibrillary pathology in Alzheimer's disease. Nat. Med. *20*, 1254–1262. https://doi.org/10.1038/nm.3700.
13. Zhang, Z., Kang, S.S., Liu, X., Ahn, E.H., Zhang, Z., He, L., Iuvone, P.M., Duong, D.M., Seyfried, N.T., Benskey, M.J., et al. (2017). Asparagine endopeptidase cleaves alpha-synuclein and mediates pathologic activities in Parkinson's disease. Nat. Struct. Mol. Biol. *24*, 632–642. https://doi.org/10.1038/nsmb.3433.
14. Chen, C., Zhou, Y., Wang, H., Alam, A., Kang, S.S., Ahn, E.H., Liu, X., Jia, J., and Ye, K. (2021). Gut inflammation triggers C/EBPbeta/delta-secretase-dependent gut-to-brain propagation of Abeta and Tau fibrils in Alzheimer's disease. EMBO J. *40*, e106320. https://doi.org/10.15252/embj.2020106320.
15. Kalcheim, C., and Le Douarin, N.M. (1986). Requirement of a neural tube signal for the differentiation of neural crest cells into dorsal root ganglia. Dev. Biol. *116*, 451–466. https://doi.org/10.1016/0012-1606(86)90146-6.
16. Pol, S.U., Lang, J.K., O'Bara, M.A., Cimato, T.R., McCallion, A.S., and Sim, F.J. (2013). Sox10-MCS5 enhancer dynamically tracks human oligodendrocyte progenitor fate. Exp. Neurol. *247*, 694–702. https://doi.org/10.1016/j.expneurol.2013.03.010.
17. Antonellis, A., Huynh, J.L., Lee-Lin, S.Q., Vinton, R.M., Renaud, G., Loftus, S.K., Elliot, G., Wolfsberg, T.G., Green, E.D., McCallion, A.S., and Pavan, W.J. (2008). Identification of Neural Crest and Glial Enhancers at the Mouse Sox10 Locus through Transgenesis in Zebrafish. PLoS Genet. *4*, e1000174. https://doi.org/10.1371/journal.pgen.1000174.
18. Ludwig, A., Schlierf, B., Schardt, A., Nave, K.-A., and Wegner, M. (2004). Sox10-rtTA mouse line for tetracycline-inducible expression of transgenes in neural crest cells and oligodendrocytes. genesis *40*, 171–175. https://doi.org/10.1002/gene.20083.
19. Krammer, H.-J., Karahan, S.T., Rumpel, E., Klinger, M., and Kühnel, W. (1993). Immunohistochemical visualization of the enteric nervous system using antibodies against Protein gene product (PGP) 9.5. Annals of Anatomy - Anatomischer Anzeiger *175*, 321–325. https://doi.org/10.1016/S0940-9602(11)80029-4.
20. Warnecke, T., Schäfer, K.H., Claus, I., Del Tredici, K., and Jost, W.H. (2022). Gastrointestinal involvement in Parkinson's disease: pathophysiology, diagnosis, and management. NPJ Parkinsons Dis. *8*, 31. https://doi.org/10.1038/s41531-022-00295-x.
21. Reyes, J.F., Ekmark-Léwen, S., Perdiki, M., Klingstedt, T., Hoffmann, A., Wiechec, E., Nilsson, P., Nilsson, K.P.R., Alafuzoff, I., Ingelsson, M., and Hallbeck, M. (2021). Accumulation of alpha-synuclein within the liver, potential role in the clearance of brain pathology associated with Parkinson's disease. Acta Neuropathol. Commun. *9*, 46. https://doi.org/10.1186/s40478-021-01136-3.
22. Ma, L.-Y., Liu, G.-L., Wang, D.-X., Zhang, M.-M., Kou, W.-Y., and Feng, T. (2019). Alpha-Synuclein in Peripheral Tissues in Parkinson's Disease. ACS Chem. Neurosci. *10*, 812–823. https://doi.org/10.1021/acschemneuro.8b00383.
23. Dugger, B.N., Hoffman, B.R., Scroggins, A., Serrano, G.E., Adler, C.H., Shill, H.A., Belden, C.M., Sabbagh, M.N., Caviness, J.N., Driver Dunckley, E., and Beach, T.G. (2019). Tau immunoreactivity in peripheral tissues of human aging and select tauopathies. Neurosci. Lett. *696*, 132–139. https://doi.org/10.1016/j.neulet.2018.12.031.
24. Xiang, J., Tao, Y., Xia, Y., Luo, S., Zhao, Q., Li, B., Zhang, X., Sun, Y., Xia, W., Zhang, M., et al. (2023). Development of an α-synuclein positron emission tomography tracer for imaging synucleinopathies. Cell *186*, 3350–3367.e19. https://doi.org/10.1016/j.cell.2023.06.004.
25. Wakabayashi, K., Mori, F., Tanji, K., Orimo, S., and Takahashi, H. (2010). Involvement of the peripheral nervous system in synucleinopathies, tauopathies and other neurodegenerative proteinopathies of the brain. Acta Neuropathol. *120*, 1–12. https://doi.org/10.1007/s00401-010-0706-x.
26. Shannon, K.M., Keshavarzian, A., Mutlu, E., Dodiya, H.B., Daian, D., Jaglin, J.A., and Kordower, J.H. (2012). Alpha-synuclein in colonic submucosa in early untreated Parkinson's disease. Mov. Disord. *27*, 709–715. https://doi.org/10.1002/mds.23838.
27. Trojanowski, J.Q., Schuck, T., Schmidt, M.L., and Lee, V.M. (1989). Distribution of tau proteins in the normal human central and peripheral nervous system. J. Histochem. Cytochem. *37*, 209–215. https://doi.org/10.1177/37.2.2492045.
28. Lionnet, A., Wade, M.A., Corbillé, A.-G., Prigent, A., Paillusson, S., Tasselli, M., Gonzales, J., Durieu, E., Rolli-Derkinderen, M., Coron, E., et al. (2018). Characterisation of tau in the human and rodent enteric nervous system under physiological conditions and in tauopathy. Acta Neuropathol. Commun. *6*, 65. https://doi.org/10.1186/s40478-018-0568-3.
29. Braak, H., Del Tredici, K., Rüb, U., de Vos, R.A.I., Jansen Steur, E.N.H., and Braak, E. (2003). Staging of brain pathology related to sporadic Parkinson's disease. Neurobiol. Aging *24*, 197–211. https://doi.org/10.1016/S0197-4580(02)00065-9.
30. Arotcarena, M.L., Dovero, S., Prigent, A., Bourdenx, M., Camus, S., Porras, G., Thiolat, M.L., Tasselli, M., Aubert, P., Kruse, N., et al. (2020). Bidirectional gut-to-brain and brain-to-gut propagation of synucleinopathy in non-human primates. Brain *143*, 1462–1475. https://doi.org/10.1093/brain/awaa096.
31. Wang, H., Chen, G., Ahn, E.H., Xia, Y., Kang, S.S., Liu, X., Liu, C., Han, M.H., Chen, S., and Ye, K. (2023). C/EBPβ/AEP is age-dependently activated in Parkinson's disease and mediates α-synuclein in the gut and brain. NPJ Parkinsons Dis. *9*, 1. https://doi.org/10.1038/s41531-022-00430-8.
32. Wang, J., Yang, X., Zeng, W., Zhang, X., Yang, X., Xu, Y., Liu, K., Zhang, Z., Xu, Y., and Cao, X. (2022). Dual Effects: Intrastriatal Injection of α-syn N103/tau N368 Preformed Fibrils Promotes Endogenous α-synuclein Aggregates in the Proximal Colon. J. Parkinsons Dis. *12*, 2097–2116. https://doi.org/10.3233/JPD-223294.
33. Johansson, M., Stomrud, E., Insel, P.S., Leuzy, A., Johansson, P.M., Smith, R., Ismail, Z., Janelidze, S., Palmqvist, S., van Westen, D., et al. (2021). Mild behavioral impairment and its relation to tau pathology in

preclinical Alzheimer's disease. Transl. Psychiatry *11*, 76. https://doi.org/10.1038/s41398-021-01206-z.

34. Bejanin, A., Schonhaut, D.R., La Joie, R., Kramer, J.H., Baker, S.L., Sosa, N., Ayakta, N., Cantwell, A., Janabi, M., Lauriola, M., et al. (2017). Tau pathology and neurodegeneration contribute to cognitive impairment in Alzheimer's disease. Brain *140*, 3286–3300. https://doi.org/10.1093/brain/awx243.

35. Sánchez-Ferro, Á., Rábano, A., Catalán, M.J., Rodríguez-Valcárcel, F.C., Díez, S.F., Herreros-Rodríguez, J., García-Cobos, E., Álvarez-Santullano, M.M., López-Manzanares, L., Mosqueira, A.J., et al. (2015). In vivo gastric detection of α-synuclein inclusions in Parkinson's disease. Movement Disorders *30*, 517–524. https://doi.org/10.1002/mds.25988.

36. Beach, T.G., Corbillé, A.-G., Letournel, F., Kordower, J.H., Kremer, T., Munoz, D.G., Intorcia, A., Hentz, J., Adler, C.H., Sue, L.I., et al. (2016). Multicenter Assessment of Immunohistochemical Methods for Pathological Alpha-Synuclein in Sigmoid Colon of Autopsied Parkinson's Disease and Control Subjects. J. Parkinsons Dis. *6*, 761–770. https://doi.org/10.3233/JPD-160888.

37. Hilton, D., Stephens, M., Kirk, L., Edwards, P., Potter, R., Zajicek, J., Broughton, E., Hagan, H., and Carroll, C. (2014). Accumulation of α-synuclein in the bowel of patients in the pre-clinical phase of Parkinson's disease. Acta Neuropathol. *127*, 235–241. https://doi.org/10.1007/s00401-013-1214-6.

38. Schneider, C.A., Rasband, W.S., and Eliceiri, K.W. (2012). NIH Image to ImageJ: 25 years of image analysis. Nat. Methods *9*, 671–675. https://doi.org/10.1038/nmeth.2089.

39. Qiu, L., Jiang, H., Yu, Y., Gu, J., Wang, J., Zhao, H., Huang, T., Gropler, R.J., Klein, R.S., Perlmutter, J.S., and Tu, Z. (2022). Radiosynthesis and evaluation of a fluorine-18 radiotracer [(18)F]FS1P1 for imaging sphingosine-1-phosphate receptor 1. Org. Biomol. Chem. *20*, 1041–1052. https://doi.org/10.1039/d1ob02225c.

40. Chen, J., Lin, Y., Huang, J., Wang, W., Wei, Y.-Y., Li, Y.-Q., Kaneko, T., and Wu, S.-X. (2013). Mammal retinal distribution of ENKergic amacrine cells and their neurochemical features: Evidence from the PPE-GFP transgenic mice. Neurosci. Lett. *548*, 233–238. https://doi.org/10.1016/j.neulet.2013.05.054.

41. Chandrasekharan, B.P., Kolachala, V.L., Dalmasso, G., Merlin, D., Ravid, K., Sitaraman, S.V., and Srinivasan, S. (2009). Adenosine 2B receptors (A2BAR) on enteric neurons regulate murine distal colonic motility. Faseb. J. *23*, 2727–2734. https://doi.org/10.1096/fj.09-129544.

42. Zhishan, L., Alcmène, C., Yung-yu, H., Mann, J.J., Kara Gross, M., Qi Melissa, Y., Dolly, O.K., Francine, C., Jacques, M., and Michael, D.G. (2011). Essential Roles of Enteric Neuronal Serotonin in Gastrointestinal Motility and the Development/Survival of Enteric Dopaminergic Neurons. J. Neurosci. *31*, 8998. https://doi.org/10.1523/JNEUROSCI.6684-10.2011.

43. Li, Z., Chalazonitis, A., Huang, Y.Y., Mann, J.J., Margolis, K.G., Yang, Q.M., Kim, D.O., Côté, F., Mallet, J., and Gershon, M.D. (2011). Essential roles of enteric neuronal serotonin in gastrointestinal motility and the development/survival of enteric dopaminergic neurons. J. Neurosci. *31*, 8998–9009. https://doi.org/10.1523/JNEUROSCI.6684-10.2011.

44. Sakata, K., Jin, L., and Jha, S. (2010). Lack of promoter IV-driven BDNF transcription results in depression-like behavior. Genes Brain Behav. *9*, 712–721. https://doi.org/10.1111/j.1601-183X.2010.00605.x.

45. Jiang, Y., Tian, Y., Feng, B., Zhao, T., Du, L., Yu, X., and Zhao, Q. (2023). A novel molecular imaging probe [99mTc]Tc-HYNIC-FAPI targeting cancer-associated fibroblasts. Sci. Rep. *13*, 3700. https://doi.org/10.1038/s41598-023-30806-6.

STAR★METHODS

KEY RESOURCES TABLE

REAGENT or RESOURCE	SOURCE	IDENTIFIER
Antibodies		
Phospho-Tau (Ser202, Thr205) Antibody (AT8)	Thermo fisher	MN1020; RRID:AB_223647
PGP9.5 Antibody	GeneTex	GTX109637; RRID:AB_1952497
TH Rabbit Polyclonal Antibody	proteintech	25859-1-AP; RRID:AB_271656
SOX10 Polyclonal Antibody	proteintech	10422-1-AP; RRID:AB_2195371
RFP Antibody	GeneTex	GTX127897; RRID:AB_2885652
Anti-Aggregated α-Synuclein, clone (5G4)	Millipore	VP1801021; RRID:AB_2716647
Anti-Tau, AEP-cleaved (N368) monoclonal	Gene Create	Customer made
Anti-α-Synuclein N103 monoclonal	Gene Create	Customer made
Anti-NeuN-Rabbit	Millipore	ABN78; RRID:AB_1080794
Anti-Glial Fibrillary Acidic Protein Antibody, clone GA5	Millipore	GTX108711; RRID:AB_2037091
Anti-mouse IgG(H + L), F(ab')2 Fragment (Alexa Fluor® 594 Conjugate)	Cell signaling	8889; RRID:AB_2716249
Anti-rabbit IgG (H + L), F(ab')2 Fragment (Alexa Fluor® 647 Conjugate)	Cell signaling	8890; RRID:AB_2714182
Chemicals, peptides, and recombinant proteins		
BSA	Sigma	9048-46-8
Triton X-100	PUMOKE	PMK05634
F0502B	Shanghai Braegen Pharmaceuticals, Inc.	N/A
F0502B precursor	Shanghai Braegen Pharmaceuticals, Inc.	N/A
Carmine Red	Sigma-Aldrich	SHBL1491
Methylcellulose	Sigma-Aldrich	M7027
ThS	Sigma-Aldrich	T1892
tetracycline hydrochloride	Merck	58346-M
Iopromide	Bayer	73334-07-3
Isoflurane	RWD Life Science	R510-22-10
Critical commercial assays		
DAB Horseradish Peroxidase Color Development Kit	ZSBIO	ZLI-9018
Anti-mouse/rabbit IHC Detection Kit	ZSBIO	PV-6000
MEGAshortscript™ T7 Kit	Thermo Fisher	AM1354
SHIELD Kit	LifeCanvas Technologies	SH-250
Experimental models: Organisms/strains		
Both Tg mice	Gempharmatech Co., Ltd	Customer design
TAU368$^{+/-}$ Tg mice	Gempharmatech Co., Ltd	Customer design
SYN103$^{+/-}$ Tg mice	Gempharmatech Co., Ltd	Customer design
Software and algorithms		
ImageJ 1.53	Schneider et al.[38]	https://imagej.nih.gov/ij/
Graph Pad Prism 8	GraphPad	https://www.graphpad.com/scientific-software/prism
FV31S-DT 2.6	Olympus	https://lifescience.evidentscientific.com.cn/zh/downloads/detail-iframe/?0[downloads][id]=847252002

(*Continued on next page*)

Continued

REAGENT or RESOURCE	SOURCE	IDENTIFIER
SMART video tracking 3.0	RWD Life Science	https://www.rwdls.com/product-solutions/life-sciences/behavior/tracing
EV screen recording	Ieway Technology	https://www.ieway.cn/
Tanon ABL X6 Caliper IVIS Lumina II	Tanon	https://biotanon.com/Product/ProductList?id=1095&type=Detail
Living Image 4.4	PerkinElmer	https://www.perkinelmer.com.cn/lab-products-and-services/resources/tissue-imaging-software-downloads.html
PMOD	Qiu et al.[39]	https://www.pmod.com/web/
Interview Fusion processing software 1.0	Mediso, Hungry	https://mediso.com/global/en/product/interview-processing-workstation/interview-fusion-processing-software

EXPERIMENTAL MODEL AND SUBJECT DETAILS

Mice

To develop a Dox-inducible gene expression system for triple models, we named them SYN103 knock-in (SYN103$^{+/-}$), TAU368 knock-in (TAU368$^{+/-}$) and double knock-in (both). A donor vector containing two cassettes, one was the tetracycline-induced SYN103 or TAU368 protein followed by RFP linked by one self-cleaving 2A peptide (P2A) under the regulation of tetracycline responsive elements (TREs; tetO), and the other was the reverse tetracycline-controlled *trans*-activator gene named rTTA3G driven by the *Sox10-MCS4* enhancer and *c-fos* minimal promotor, the donor vector containing the inserted Gt(ROSA)26Sor locus and H11 locus using the CRISPR−Cas-9 technique (generated by Gempharmatech Co., Ltd., China). The gRNAs were produced by *in vitro* transcription using a MEGAshortscript T7 kit. A donor plasmid in which the cassette was flanked by two 1.0 kb homologous arms was used as the repair template for homologous recombination, and gRNA and donor vector with the purified Cas9 proteins were injected into the mouse embryos in the C57BL/6JGpt genetic background for genetic editing. PCR and genome sequencing identified the positive recombination founder mice.

To activate the Tet-on system, mice at 2 months old were treated with 10 mg/kg tetracycline orally dissolved in PBS for 8 weeks. The control mice were heterozygous. Both mice were treated for 8 weeks with only PBS by oral gavage. Animal care and handling were performed according to NIH animal care guidelines and approved by the Institutional Animal Care and Use Committee of the Fourth Military Medical University. Mice were housed in a room maintained at a constant temperature and on a 12-h light/dark cycle (light from 08:00 to 20:00). Water and food were available *ad libitum*. All animals were randomly allocated to the different experimental conditions used in this study.

METHOD DETAILS

Immunofluorescence staining

For immunofluorescence staining of frozen gut and brain sections, after perfusion, the mouse brain, jejunum, ileum, cecum, and colon tissues were fixed with 4% paraformaldehyde and then 30% sucrose in PBS followed by PBS-Triton (3% BSA, 0.1% Triton X-100) solution. The gut and brain were cut into 30-μm-thick sections on a cryotome. The mucosa, submucosa, and inner muscle layer were separated from the outer longitudinal layer for whole mount intestine myenteric plexus preparation. The sections and intestinal plexus were incubated overnight with the primary antibodies listed in the key resource tables. After washing three times with PBS, the sections were incubated with the fluoro-conjugated secondary antibody listed in Key resource tables for 2 h. For ThS or F0502B staining, after finishing secondary antibody staining, rinse the sections with PBS three times, then apply the ThS or F0502B at 50 μM with 50% EtOH to the sections for 10–15 min in the dark; rinse the sections with distilled water. After DAPI staining for 10 min, the sections were washed with PBS and covered with mounting solution. The sections were observed under an Olympus FV3000 microscope and VS200 slide scanner. For histological and cell mapping studies, coronal sections were stained and immunoreactive inclusions/cells and neurites were mapped at multiple rostrocaudal levels corresponding to −0.86 mm, −2.18 mm, −2.80 mm, −4.72 mm, −5.40 mm, −6.36mm relative to bregma. Images were captured using a VS200 (Olympus) and ImageJ was used to mark the positive neurons and draw the diagram.

Immunohistochemical staining

Freshly dissected heart, liver, spleen, lung, and kidney tissues were fixed with 10% formalin for 24 h and dehydrated with alcohol. The tissues were cleared with xylene and immersed in paraffin. The paraffin-embedded tissue blocks were sectioned at 5 μm thickness. The slides were deparaffinized in xylene and transferred to different concentrations of alcohol for recovery. The sections were incubated with 3% H_2O_2 for 10 min and treated with 10 mM citrate buffer, pH 6.0, for antigen retrieval for 10 min at 95°C. Sections were

blocked with 1% BSA and 0.3% Triton X-100 for 1 h and incubated with α-Syn N103 (1:200) and Tau N368 (1:200) at 4°C overnight. The signal was developed using an IHC detection kit (ZSBIO).

Cell quantification

For quantification analysis, the methods were described previously.[40] Three sections were selected from each animal sample (usually n = 3–4), and 4 randomly selected areas of interest within each section were analyzed to determine positive cells per square millimeter. Cells with clear DAPI staining were counted. For colocalization analysis, over 50% of the co-stained cells were counted.

Stereological cell quantification

The number of TH + cells in midbrain sections was manually determined from the maximal projection confocal images. Boundaries of the SNc were determined by TH signal threshold detection using ImageJ and manually excluding non-SNc regions within the section. The density was determined by quantifying the number of cells per SNc volume (area multiplied by the thickness of the slice). Analyses of immunohistochemical signals were performed in ImageJ. ROIs were drawn as delineated by the presence of the TH + signal specific to the region and the integrated density was measured. Integrated densities were calculated per unit area.

3D-whole-brain and colon imaging

Nuohai Life Sciences Co., Ltd. performed whole-brain and colon clearing and imaging through a contracted service. Briefly, PFA-fixed samples were incubated in SHIELD-OFF solution (freshly prepared using an SHIELD kit and kept on ice) at 4°C with shaking for 4 days, followed by SHIELD-ON solution at 37°C with shaking for 24 h. The samples were delipidated by using the stochastic electrotransport instrument SmartClear II Pro (LifeCanvas Technologies, MA, USA) and washed with PBS for 2 days. Then, the cells were immunolabeled with α-Syn N103 or Tau N368 followed by secondary fluorescent-conjugated antibodies using SmartLabel electrophoresis (LifeCanvas Technologies, MA, USA). The fluorescence images were acquired with a Nuohai LS 18 Light Sheet Microscope (Nuohai Life Science (Shanghai) Co., Ltd). For imaging at 4× zoom effective magnification, each sample was scanned by 4-tiles light sheets axially at a 3.5 μm Z-step size to image the whole sample in 3D.

Gastrointestinal motility assays

Stool water content was measured in mice as described previously.[41] The mice were placed in a transparent cage for 1 h, and the stool pellets were collected immediately and sealed in tubes. Then, the samples were weighed to obtain wet weights and dried overnight to obtain dry weights. Water contents were calculated as percentages. The red carmine dye test was used to measure the intestine emptying time.[42] Briefly, 300 μL of 6% carmine red was suspended in 0.5% methylcellulose, and the mice were administered the solution by gavage. The time at which the gavage took place was recorded as T_0. Stool pellets were monitored every 10 min. Total intestine emptying time was recorded as the interval between T_0 and the time of the first observance of carmine red in the stool. Gastric emptying was studied as previously described.[43] Briefly, the animals were anesthetized with isoflurane. A glass bead (3 mm in diameter) was pushed into the colon 2 cm away from the anal verge. The time required for the expulsion of the glass bead was recorded as an estimate of colonic motility.

Vagotomy

The mice were anesthetized by injecting 1% pentobarbital sodium. The abdominal cavity was cut open, and the diaphragm was dissected carefully to expose the vagus nerve. From the point where the esophagus and stomach connect to the diaphragm (2–3 mm above the cardia), the connective tissue around the stomach and the covered blood vessels (common carotid artery) were carefully separated from the 4–6 mm section of the branch of the stomach and then resected.

Rotarod test

Mice were trained for 3 days using the Rotarod (San Diego Instruments). On the first day, the mice were trained at a slow rotational speed (5 rpm) for a maximum of 5 min three times. On the second day, the mice were trained at 10 rpm for a maximum of 10 min three times. On the third day, the rotational speed was modulated from 5 rpm to 20 rpm at a rate of 0.1 rpm/s. On the test day, the rotational speed of the rotarod was modulated from 5 rpm to a maximum of 40 rpm. It was gradually increased during the trial at a rate of 0.1 rpm/s. Three trials of the latency to fall and the speed were recorded.

Tail suspension test

Mice were suspended by placing the free end of the tape on the suspension bar. The behaviors of the mice were recorded for 8 min, and the immobilization time percentage was analyzed.

Novel object recognition test

For habituation, mice were placed in the open field and allowed to explore for 10 min freely. On the next day, two objects were placed in opposite corners, and mice were placed in the middle of the open field to freely explore for 10 min. On the test day, one object was replaced with a novel object, and the mice were allowed to explore for 10 min. The time spent exploring the novel object was analyzed, and the discrimination index was calculated as (novel time-old time)/(total exploring time)*100%.

Water maze test

Mice were trained in a round, water-filled pool (120 cm in diameter) with four different cues on the surface. The water was dyed white, and the 9 cm platform was placed 1 cm below the surface. The pool was divided into four-quarters. Each mouse was given 4 trials/day for 4 consecutive days with a 30-min interval. The latency time and swimming speed were recorded by using a video tracking system (SMARTBasic, Panlab, Spain). If the mouse could not locate the platform within 60 s, it was placed on the platform for 10 s and then returned to its cage by the experimenter. On the last test day, the platform was removed, and the percentage of time spent in the platform quadrant was measured over 60 s.

Open field test

The mouse was placed into the center of an open field (40 cm × 40 cm × 40 cm) and allowed to explore for 10 min under dim light. The apparatus was thoroughly cleaned with diluted 10% ethanol between each trial.

A video tracking system (SMART 3.0 software) was used to record the distance traveled to measure locomotor activity. The time spent in and entries into the center were measured as an anxiolytic indicator.[44]

In vivo and *ex vivo* imaging of the brain and the GI tract

To evaluate the effects of F0502B on α-Syn or Tau aggregation *in vivo* and e*x vivo*, 10 mg/kg F0502B or ThS was intravascularly injected into the tail. After 20 min, the mice were anesthetized by gas anesthesia and then placed into the imaging system in the lateral position using a small animal optical molecular imaging system (IVIS Imaging Spectrum System, Caliper Life Sciences, Hopkinton, MA). After *in vivo* imaging, the brain and total GI tract were dissected, and fluorescence signals were captured at 488 nm. Signal intensity was quantitatively assessed by measuring the signal intensity from an equal-sized ROI of the tissues or brain/GI areas in the control, TAU368$^{+/-}$ and SYN103$^{+/-}$ groups using Living Image 4.4 software (IVIS Imaging Spectrum System, Caliper).

Radiochemistry

^{18}F-F0502B was synthesized by a one-pot two-step method using an AllinOne universal synthesizer. The synthetic route and schematic diagram were described in the supplementary materials (Figures S12A and S12B). Firstly, the tosylate precursor through an SN2 displacement with [^{18}F] fluoride. The ^{18}F-F0502B was then obtained by hydrolysis with hydrochloric acid and purified by isocratic semi-preparative radio-HPLC (Waters SunFire C18 column, 250 mm × 10 mm, 5 μm, eluent 55% CH_3CN and 45% H_2O containing 10 mM NH_4OAc, flow rate 4 mL/min). The identity of the ^{18}F-F0502B was verified and established by comparing the retention times with the corresponding unlabeled compounds, using co-injection HPLC analysis (Agela Venusil MP C18 column, 250 mm × 4.6 mm, 5 μm, eluent: 65% CH_3CN and 35% H_2O containing 10 mM NH_4OAc, flow rate: 1 mL/min).

Lipophilicity and *in vitro* stability

The lipophilicity of ^{18}F-F0502B was evaluated by distribution coefficient ($logD_{7.4}$). In brief, determined by measuring the distribution of the radiotracer between 1-octanol and potassium phosphate buffer (PBS, 0.05 mol/L, pH 7.4) using the shake-flask method according to the previously reported methods.[45] *In vitro,* stability of ^{18}F-F0502B in saline at room temperature and in mouse serum at 37°C were determined by radio-HPLC within the incubation time of 4 h.

Micro-PET/CT imaging

One hour before imaging, 200 μL of Iopromide was administered orally for CT contrast of the gastrointestinal tract. Immediately before imaging, 200 μL of Iopromide was administered orally for large-intestine contrast and the mice were anesthetized with 2% isoflurane. Throughout the experiments, anesthesia was maintained by adjusting the isoflurane content (0.6%–2%) to ensure a respiratory rate in the range of 80–100/min. SYN103$^{+/-}$, Both and control mice were used for *in vivo* ^{18}F-F0502B imaging with a micro-PET/CT system (Mediso, Hungary). Mice were anesthetized by with isoflurane and injected with 11.1 MBq of ^{18}F-F0502B via the tail vein. Dynamic ^{18}F-F0502B micro-PET/CT scans were acquired within 5–65 min post-injection after the mice were placed prone on the micro-PET/CT acquisition bed, with the following parameters (PET: 1–5 coincidence mode, 5 ns coincidence time windows; CT: SemiCircular scan, 180 projections, 55kVp X--ray energy, 600ms exposure time and maximum FOV of Zoom). The PET/CT images were iteratively reconstructed every 3 min for the first 15 min and followed by every 5 min, using a standard ordered-subset expectation maximization (OSEM) method (Tera-Tomo 3D, Voxel size: 0.4; 4 iterations, 6 subsets; filter type of Cosine, 40 × 40 × 40 mm volume size, 140 × 140 × 140 μm voxel size, 284 × 284 × 284 voxels). The PET/CT images were analyzed using the Interview Fusion 1.0 (Mediso, Hungry) software. The SUV (Standardized uptake value) -time curve is obtained by sketching the region of interest (ROIs). SUV is calculated as a ratio of tissue radioactivity concentration (kBq/mL)/administered dose (MBq)/body weight (kg).

Autoradiography

At 20 min post-injection, animals were sacrificed by cervical dislocation under anesthesia. GI and brain were extracted rapidly, the GI track was washed 3 times with PBS and dried, and the brain was snap-frozen in liquid nitrogen and then sliced using cryostat (Leica CM1860 UV). Then, mounted different GI tract parts and brain slices into microscope slides, and exposed to a phosphor-imaging screen. Autoradiography images were obtained and analyzed using Biosystems (Azure, USA).

Biodistribution

All mice were anesthetized by isofluorane inhalation and injected with radiotracer ^{18}F-F0502B (about 740 kBq, 100 μL) via bolus injection through a tail vein. Animals were sacrificed by cervical dislocation under anesthesia 20 min post-injection (n = 3 each). Samples of blood, brain regions, different GI tract parts, and other major organs harvested rapidly, weighed and counted in a gamma-counter (WIZARD 2470, PerkinElmer, USA). The percentage of injected dose per gram of wet tissue (% ID/g) was calculated by a comparison of the tissue count to suitably diluted aliquots of the injected radiotracer as counting standards.

QUANTIFICATION AND STATISTICAL ANALYSIS

All data are expressed as means ± SEM from three or more independent experiments, and the significance level between the two groups was assessed with Student's t test. For more than two groups, two-way ANOVA followed by LSD post hoc test was applied. A p value <0.05 was considered to be statistically significant. The detailed statistical data can be found in Mendeley data: https://data.mendeley.com/datasets/dfmw8fvxc2/1.